Mesoscale Variability in Denmark Strait: The PV Outflow Hypothesis*

MICHAEL A. SPALL AND JAMES F. PRICE

Department of Physical Oceanography, Woods Hole Oceanographic Institution, Woods Hole, Massachusetts

(Manuscript received 22 January 1997, in final form 28 October 1997)

ABSTRACT

The outflow through Denmark Strait shows remarkable mesoscale variability characterized by the continuous formation of intense mesoscale cyclones just south of the sill. These cyclones have a diameter of about 30 km and clear signatures at the sea surface and in currents measured near the bottom. They have a remnant of Arctic Intermediate Water (AIW) in their core.

The authors' hypothesis is that these cyclones are formed by stretching of the high potential vorticity (PV) water column that outflows through Denmark Strait. The light, upper layer of the outflow, the East Greenland Current, remains on the surface in the Irminger Sea, while the dense overflow water descends the east Greenland continental slope. The midlevel waters, mostly AIW, could thus be stretched by more than 100%, which would induce very strong cyclonic relative vorticity.

The main test of this new hypothesis is by way of numerical experiments carried out with an isopycnal coordinate ocean model configured to have a marginal sea connected to a deep ocean basin by a shallow strait. An outflow is produced by imposing buoyancy forcing over the marginal sea. If the buoyancy forcing is such as to produce a single overflow layer (analogous to the overflows through the Strait of Gibraltar and the Faroe Bank Channel), then the resulting overflow is slightly time dependent. If the buoyancy forcing is such as to produce both a deep overflow and a midlevel outflow (analogous to the AIW), then the resulting outflow is highly time dependent and develops intense midlevel cyclones just south of the sill where the dense overflow water begins to descend the continental slope. The cyclones found in the numerical solutions have time and space scales set by the midlevel outflow transport, the bottom slope, and the deep stratification. Their scales and structure are roughly consistent with the cyclones observed south of the sill in Denmark Strait.

High PV outflow through Denmark Strait is a result of the large-scale wind and buoyancy forcing over the Norwegian–Greenland Sea and Denmark Strait's location on a western boundary. So far as we know, this configuration and this specific form of mesoscale variability are unique to Denmark Strait.

1. Overflows and outflows

Most deep-water masses originate as an overflow from a nearly landlocked marginal sea having a cold or dry climate, examples considered here are the Norwegian–Greenland Sea and the Mediterranean Sea (Warren 1981; Killworth 1983; Whitehead 1989). The overflow waters from these seas are the (topographically) concentrated result of air–sea interaction over the entire marginal sea basin and they have highly anomalous density and potential vorticity where they first enter the open ocean. The Mediterranean overflow water has a density anomaly (excess) of about 1.4 kg m^{-3} with respect to North Atlantic Central Water, and the Denmark Strait overflow water from the Norwegian–Greenland Sea has an initial density anomaly of about 0.4 kg m^{-3} (Smith 1976) with respect to Irminger Sea water. Even the smaller density difference represents an enormous store of potential energy that is released as the overflow currents descend into the open ocean, and overflow currents are vigorous and highly dissipative (Price et al. 1993). Most of their energy appears to be lost to bottom friction (Johnson et al. 1994; Baringer and Price 1997), but diapycnal mixing is important in some respects, and mesoscale variability may be as well (Smith 1976; Jiang and Garwood 1996).

In this paper we examine the mesoscale dynamics of an overflow with an emphasis on processes that may lead to variability. Our goal is to understand better the remarkable variability that has been observed in the Denmark Strait overflow, beginning with the pioneering observations of Cooper (1955) taken along the east Greenland continental slope (Figs. 1 and 2). Cooper found that the overflow water was contained largely within mesoscale ''boluses,'' that moved southwestward along the slope. Further evidence of this variability came from Worthington's (1969) measurements of currents near the sill west of Iceland, which showed that the

* Woods Hole Oceanographic Institution Contribution Number 9407.

Corresponding author address: Dr. Michael A. Spall, Department of Physical Oceanography, Woods Hole Oceanographic Institution, 360 Woods Hole Road, Woods Hole, MA 02543.
E-mail: mspall@whoi.edu

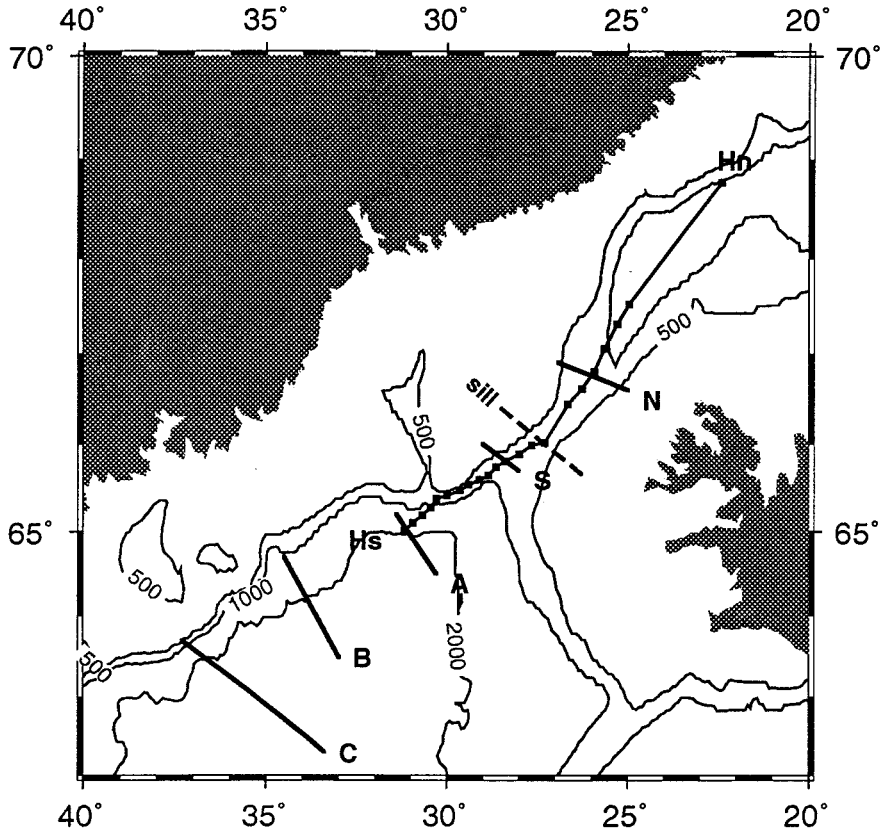

FIG. 1. Denmark Strait and the sites of historical observations referred to in the text. S and N are the current meter arrays of Ross (1984) analyzed by Smith (1976); A, B, and C are arrays deployed by Dickson and Brown (1994) to measure the overflow transport. The alongstream section Hs to Hn is a hydrographic section made during the Hudson 1973 expedition reported by Ross (1982).

overflow was highly variable at periods of several days. The peak overflow currents were up to 150 cm s^{-1}, or roughly twice the long-term mean, and coincided with the coldest overflow. Thus the boluses seen by Cooper appeared to have an origin at least as far upstream as the sill. Worthington was unable to correlate this variability with wind or surface pressure variations, which suggests that it may arise from an instability of the overflow itself (Smith 1976).

Other major overflows appear to be much less variable at mesoscale frequencies. The Norwegian–Greenland Sea overflow through Faroe Bank Channel has similar mean speeds and produces a similar bottom water type (Crease 1965). Mesoscale variability within the Faroe Bank Channel overflow is much less than the mean (Saunders 1990; Borenas and Lundberg 1988) [though the upper-layer inflow through Faroe Bank Channel shows considerable temporal variability that appears to be typical of the region (Poulain et al. 1996)]. The Mediterranean overflow in the eastern Gulf of Cadiz exhibits little variability at these frequencies (Heezen and Johnson 1969; Baringer and Price 1997) [though it forms mesoscale anticyclones in the western Gulf of Cadiz (Prater and Sanford 1994)]. Foldvik et al. (1985) described overflow currents observed in the Filchner Depression of the southern Weddell Sea, and there too the mesoscale variability is moderate.

a. Goals and outline

One step toward a useful understanding of overflows and outflows would be to answer

> What is the source of the mesoscale variability in Denmark Strait?

and the closely related question

> Why is Denmark Strait especially energetic?

In this paper we develop what is called the PV outflow hypothesis, which, in brief, argues that mesoscale variability follows from the adjustment of the high PV outflow water column to a low PV oceanic environment. A review of the circulation and hydrography in Denmark Strait shows the origin of this hypothesis (the next section) and an examination of the observed structure of the eddy variability provides some clues to the under-

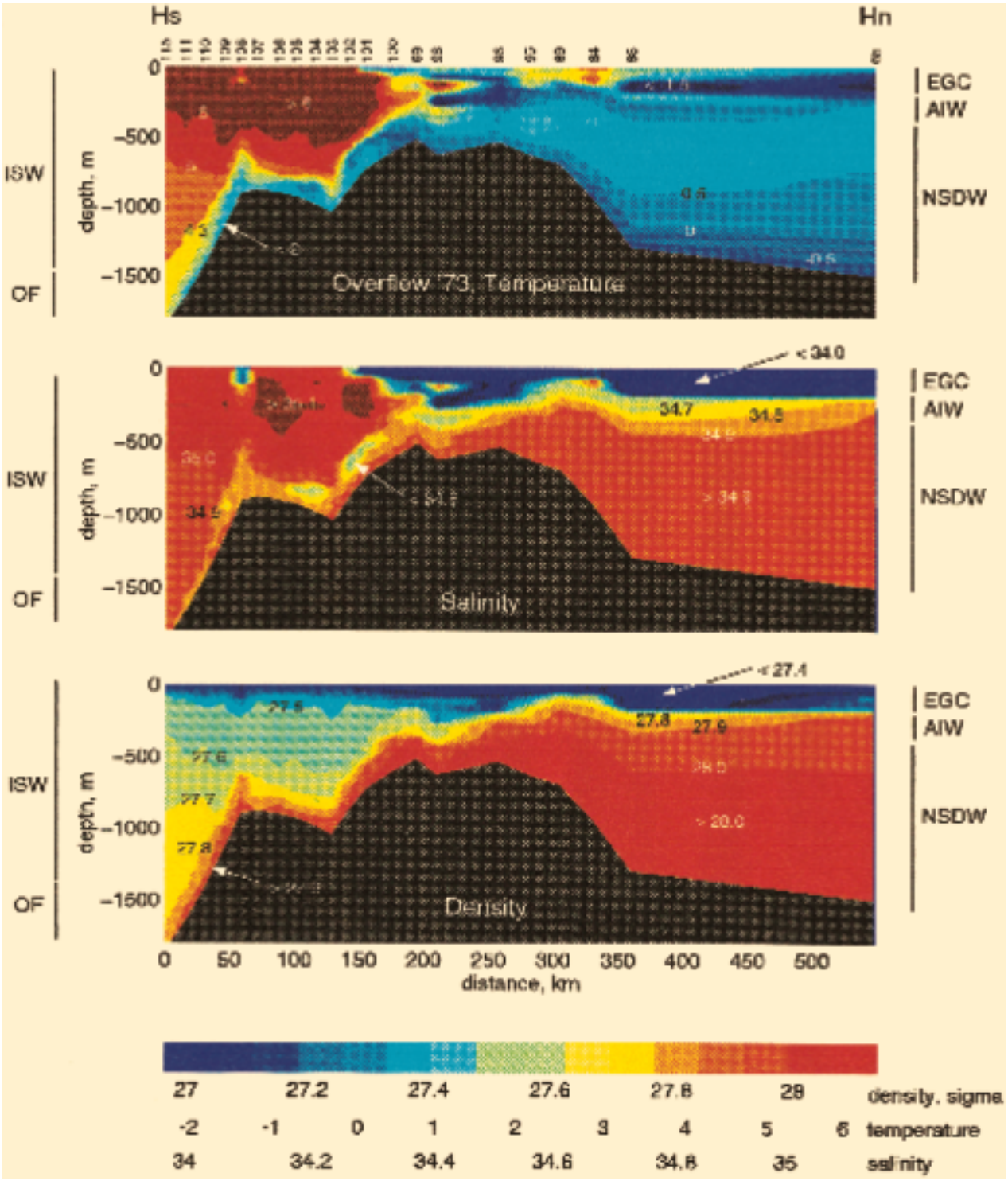

FIG. 2. A hydrographic section along the path of the Denmark Strait outflow made as part of the Overflow '73 Expedition reported by Ross (1982) (see also Bruce 1995). This is evidently the only well-sampled hydrographic section along the path of the Denmark Strait outflow. Within the Norwegian–Greenland Sea there are three distinct water masses that outflow through Denmark Strait; EGC is the fresh and cold East Greenland Current, AIW is Arctic Intermediate Water, and NSDW is Norwegian Sea Deep Water. South of the sill there are two water masses; ISW is warm and salty Irminger Sea Water and OF is overflow water, a mixture of NSDW, AIW, and ISW. The flow of the ISW in this section is not known; OF flows along and down the topography. The AIW is near the density crossover evident in Fig. 3. North of the sill there is a continuous layer of AIW present at depths of about 150–250 m. South of the sill, the AIW is split vertically. The upper part of the AIW layer disappears from the section (probably advected to the west of the section as is the EGC water mass), while the lower part is broken up into discrete boluses whose width and separation are consistent with the cyclones seen in surface IR imagery (Bruce 1995).

lying process (the remainder of this section). The main test of the hypothesis is by way of numerical simulations. The numerical ocean model and its configuration and forcing are summarized in section 2. The mean and time-dependent behavior of a multilayer outflow are discussed in section 3. A variety of numerical experiments have been carried out to isolate physical processes (section 4) and to describe the effects of differing outflow conditions or bottom slope (section 5). A comparison with other theoretical, numerical, and laboratory studies of density currents is in section 6. The results are briefly summarized in section 7.

b. A review of the Denmark Strait outflow

The notable difference in mesoscale variability between the overflows could arise from one or several sources in combination, likely candidates being the local bottom topography and the structure of the overflow/outflow[1] circulation. Denmark Strait is considerably wider than Faroe Bank Channel or the Strait of Gibraltar, and this could have important consequences for the exchange process and for mesoscale variability. Downstream of the sill the bottom topography appears unremarkable, and for that reason we have not pursued the kind of detailed simulations required to assess the effects of realistic bottom topography. A review of the circulation in these three overflows reveals similarities and differences that do seem to be significant and are the starting point for the present study.

1) LARGE-SCALE CIRCULATION AND HYDROGRAPHY

The circulations through the Faroe Bank Channel and the Strait of Gibraltar are similar in that they are both two-layer, density-driven exchange flows: a dense and nearly homogeneous lower layer overflows from the marginal sea and is replaced by a lighter, more or less stratified inflow of oceanic water. Within Denmark Strait the dense lower layer overflows as in the other cases, but there is also an outflow in the upper and midlevels of the water column (Ross 1984; Mauritzen 1996, and references therein) (Figs. 2 and 3) (there is a weak inflow on the eastern side of the Strait).

This unusual outflow structure would appear to be a direct consequence of Denmark Strait's location on a western boundary, and that it is one of several outlets from the Norwegian–Greenland Sea to the North Atlantic (the other being across the Iceland–Scotland Ridge and Faroe Bank Channel). Thus the net flow through Denmark Strait need not balance volume even approximately (as does the net flow through the Strait of Gibraltar, for example). The outflow has both a wind-driven component, the East Greenland Current (EGC), which is the western boundary current for the wind-driven subpolar gyre in the Norwegian–Greenland Sea, and a density-driven component (judging from Fig. 2) composed of Arctic Intermediate Water (AIW) and Norwegian Sea Deep Water. EGC water is less dense than the surface layer in the Irminger Sea and the EGC can continue southward along the east Greenland continental slope without having to undergo a qualitative adjustment. The densest overflow components, lower Arctic Intermediate Water (1AIW, which has properties $0 \leq \Theta \leq 2°\text{C}$, $34.9 \leq S \leq 35.0$ psu, and $27.85 \leq \sigma_\theta \leq 28.05$ kg m^{-3}) and Norwegian Sea Deep Water ($\theta \leq 0°\text{C}$, $S \approx 34.92$ psu, and $\sigma_\theta \approx 28.05$ kg m^{-3}) (water mass definitions follow Mauritzen 1996) are sufficiently dense that they could descend to the deep sea floor of the northern North Atlantic. The densest overflow waters clearly do descend the Greenland continental slope (Fig. 2), while the East Greenland Current necessarily remains on the surface. As the upper and lower layers of the outflow diverge, it would appear that the midlevel of the water column could be stretched substantially (Fig. 3) (the kinematics of this stretching are examined in section 4). The midlevel water is mainly upper Arctic Intermediate Water, (uAIW, which has properties $0 \leq \Theta \leq 2°\text{C}$, $34.7 \leq S \leq 34.9$ psu, and $27.7 \leq \sigma_\theta \leq 27.85$ kg m^{-3}). The uAIW has a thickness of about 100 m within the Norwegian–Greenland Sea, while the same range of density has a thickness of O(200–500 m) in the Irminger Sea (Figs. 2 and 3). Stretching by even a small fraction of this thickness difference would be accompanied by very large cyclonic relative vorticity. The overflow water, which remains on the bottom, need not be stretched (or compressed) in the same way, though as we will describe in the next section, mesoscale variability is observed throughout the water column.

This review of the circulation and hydrography in Denmark Strait has led to the so-called PV outflow hypothesis and three corollaries:

Summary of the observations: Mesoscale variability is unusually strong near and downstream of the sill in Denmark Strait. Denmark Strait also appears to be unique in that the large-scale wind and buoyancy forcing produce a high PV (highly stratified) outflow throughout the water column.

Hypothesis: Mesoscale variability near the sill in Denmark Strait is generated during the adjustment of the high PV outflow to the low PV oceanic environment.

Corollary 1: Mesoscale variability should be cyclonic and high Rossby number as a result of intense vortex stretching.

Corollary 2: Vortex stretching should occur mainly in the *mid*water column, roughly $27.7 \leq \sigma_\theta \leq 27.8$ kg m^{-3}, which should show the maximum response of currents.

[1] By *over*flow we mean the density current that remains on the bottom for some distance downstream of the sill, while *out*flow implies only that the current is directed from the marginal sea and toward the open ocean.

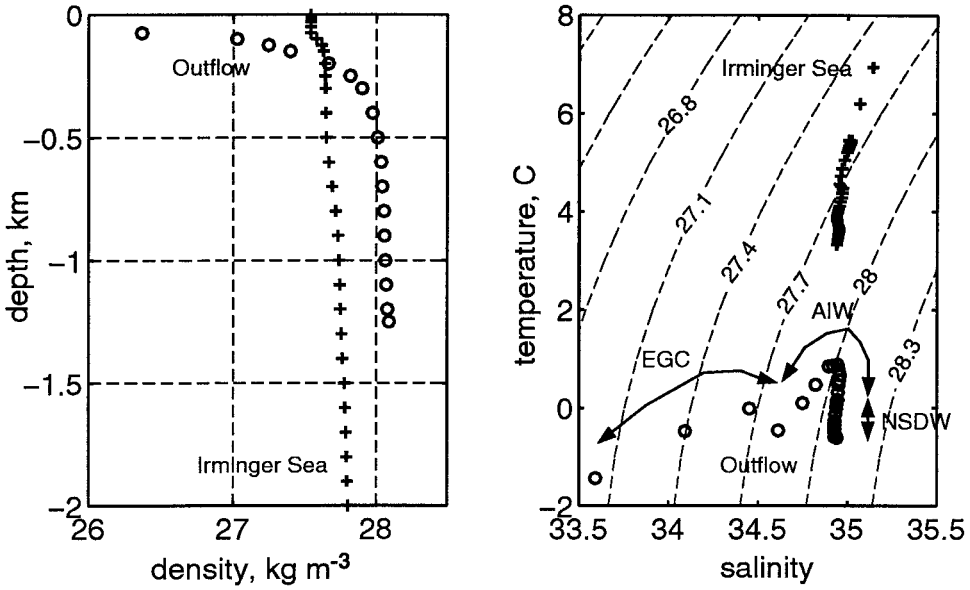

FIG. 3. Density profiles and *T/S* diagram for the northern Denmark Strait (open circles, labeled ''outflow'') and in the northern central Irminger Sea (crosses, labeled ''Irminger Sea'') [taken from the climatology of Lozier et al. (1995)]. Note that the outflow water has a larger top to bottom density range than does the Irminger Sea water. Outflow water that is less dense than about 27.6 kg m^{-3} will remain on the surface in the Irminger Sea, while outflow water denser than about 27.8 kg m^{-3} will remain on the bottom. The crossover density occurs within the density range of upper Arctic Intermediate Water.

All of the outflow water masses could be said to have a common origin in the warm and saline Atlantic inflow to the Norwegian–Greenland Sea. The inflow has *T/S* characteristics much like the warmest Irminger Sea water. The Atlantic water is cooled significantly in the Norwegian–Greenland Sea, which would tend to decrease PV and stratification, but it also gains fresh water from the surface and from runoff and ice melt. The Atlantic water becomes differentiated by salinity as it flows along different paths through the Norwegian–Greenland Sea and Arctic Ocean (Mauritzen 1996). The East Greenland Current acquires a comparatively low salinity from the Arctic Ocean and as it flows along the east Greenland ice shelf. Norwegian Sea Deep Water appears to be formed somewhere in the central Norwegian–Greenland Sea without gaining much fresh water. The Denmark Strait outflow has high PV mainly because of these salinity variations.

Corollary 3: This mechanism is *not* expected to be effective in overflows produced by two-layer exchange flows, for example, through Faroe Bank Channel and the Strait of Gibraltar.

The third corollary is the clue that led to the hypothesis and is thus not a prediction. The first and second corollaries *are* predictions, and are distinct from the kind of variability predicted by previous theories of this variability (by Smith 1976 and Jiang and Garwood 1996). They can be checked, partially, against the known characteristics of Denmark Strait variability.

2) MESOSCALE VARIABILITY

A variety of observations from Denmark Strait show one or another aspect of the mesoscale variability; Bruce (1995) pointed out that most eddy characteristics seen in in situ observations are consistent with his satellite IR observations of mesoscale cyclone formation just south of the sill. We too infer that mesoscale cyclones are the dominant mode of mesoscale variability near and just south of the sill.

Eddy scales and translation. All of the moored array data from sites near the sill exhibit very strong current variability at a period of several days, which is by far the most energetic timescale (Worthington 1969; Ross 1982; Smith 1976; Aagaard and Malmberg 1978, unpublished manuscript[2]; Dickson and Brown 1994). Satellite images indicate a very similar timescale for cyclone formation (Bruce 1995). This is probably the most robust evidence that mesoscale variability is mainly cyclonic, but there is other evidence from hydrographic properties noted below. The dominant eddy period increases downstream of the sill (Dickson and Brown 1994) and is about five to seven days at the arrays B or C of Fig. 1.

The cyclones observed in satellite imagery and drifter trajectories have a diameter of about 30 km (Bruce 1995) and an azimuthal current speed of about 50 cm s^{-1} (Krauss 1996). Hence their Rossby number is $O(1)$.

The cyclones move to the southwest at a speed of about 30 cm s^{-1}. The large-scale mean flow along the

[2] Low-frequency characteristics of the Denmark Strait overflow. ICES, C.M. 1978/C:47, 22 pp.

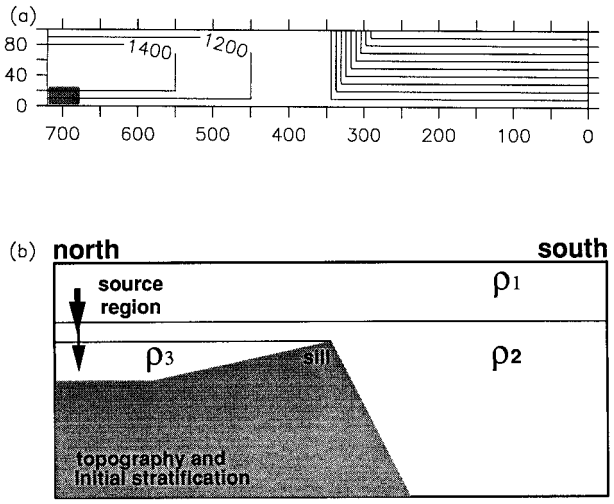

FIG. 4. Model configuration (a) domain and bottom topography (source region for the overflow waters is shaded) and (b) north–south vertical section indicating bottom topography, initial stratification, and buoyancy forcing region.

east Greenland slope is also southwesterly, but there is some evidence that the eddies move faster than the surrounding mean flow by roughly 10–30 cm s^{-1} (Krauss 1996). Their path is inclined toward greater water depth at a rate of about $\partial H/\partial s \approx 3 \times 10^{-3}$, where H is water depth and s is the distance downstream (estimated from data in Bruce 1995, Fig. 4).

Alongstream variation of amplitude. A subjective impression from the satellite imagery (Bruce 1995) is that these cyclones form rather abruptly in the vicinity of 66°N, 29°W, about 75 km south of the sill and where the overflow encounters a rapidly deepening bottom. The eddy amplitude seen in moored array data has a similar spatial structure. The eddy amplitude is comparatively low at about 75 km north of the sill (Smith 1976; the array location N of Fig. 1) and has a maximum somewhere between the sill and very roughly 150 km south of the sill. The eddy amplitude decreases farther downstream along the Greenland continental slope [judging from array measurements by Dickson and Brown (1994) along lines A, B, and C of Fig. 1]. This distribution of eddy amplitude taken together with Worthington's negative result for external forcing suggests that mesoscale variability is intrinsic to the current itself, that is, that it results from an instability or adjustment process that must occur very rapidly (within about one eddy period following a parcel) as the outflow crosses the sill west of Iceland.

Vertical structure. Smith's (1976) analysis of array data from site S just south of the sill (Fig. 1) showed that the eddy variability had an almost uniform phase with depth (though the available measurements did not include the surface layer). Aagaard and Malmberg (1978, personal communication) observed that when boluses of dense bottom water passed through their current meter array (just south of the S array of Fig. 1) the velocity then increased with height above the bottom. This is consistent with the passage overhead of cyclonic eddies (anticyclonic eddies would result in the current amplitude increasing toward the bottom) but, given the presence of a horizontally sheared mean flow, not conclusive. There was little phase change with depth during these events, suggesting an almost barotropic vertical structure within the eddies. Krauss (1996) reached a similar conclusion from an analysis of hydrographic and drifter observations.

The eddy variability has a current maximum at a depth well above the maximum of the mean flow, which is within the overflow layer and distinctly bottom trapped. Downstream of the sill (array A of Fig. 1) the eddy maximum is above the *on*shore side of the core of the deep overflow layer (Dickson and Brown 1994).

Water mass properties. Bruce (1995) analyzed several hydrographic sections taken along the array line S (Fig. 1) while current meters were in place (Ross 1982). The sections showed very large variability in the thickness of the overflow layer that were positively correlated with transport variations. During one such event the transport of overflow water (potential temperature less than 2°C) was about 5×10^6 m^3 s^{-1}, or roughly twice the long-term mean. There was low salinity core of AIW at middepths (depths 200–500 m, potential density $\approx$ 27.8 kg m^{-3}, salinity $\approx$ 34.6–34.8 psu) and a nearly homogeneous overflow water mass about 200 m thick (salinities of 34.8–34.9 psu and a potential density about 28.0 kg m^{-3}). This pulse of overflow was accompanied by strong cyclonic shear throughout the water column (peak azimuthal speeds of 60 cm s^{-1}). By contrast, periods of low overflow transport had much thinner AIW layers, and weaker or vanishing cyclonic relative vorticity.

Hydrographic data downstream of the sill show the presence of mesoscale eddies (or boluses) that move southwestward along the east Greenland continental slope (Cooper 1955). Bruce (1995) and Krauss (1996) noted that these hydrographic features have horizontal scales that are consistent with the cyclones seen in sea surface imagery and in surface drifter data. The θ/S within these cyclones shows a distinct, low salinity remnant of AIW (Fig. 2), consistent with the event described in the paragraph above.

A summary of these eddy properties is listed in Table 1. Of these, the most distinctive are perhaps the last two—the sign of the eddy vorticity and the comparison to other overflows—which are largely qualitative.

2. The numerical ocean model

The cumulative weight of the observations from Denmark Strait makes a fairly strong prima facie case that the mesoscale variability is associated primarily with

TABLE 1. Characteristics of mesoscale variability observed near and to the south of the sill in Denmark Strait.

1) *Formation.* Eddy formation occurs rapidly just south of the sill and goes on more or less continuously. (Smith 1976; Bruce 1995).
2) *Eddy diameter.* Eddies observed in SST and hydrography have a diameter of about 30 km and a separation between eddy centers of about 70 km. (Cooper 1955; Bruce 1995).
3) *Period.* The dominant eddy period observed in currents in situ is about 2–3 days near the sill and increases downstream. (Worthington 1969; Smith 1976; Dickson and Brown 1994).
4) *Translation velocity.* Eddies move to the southwest at approx. 30 cm s^{-1} (due in part to advection by large-scale mean flow). The mean path of the surface signature is inclined toward deeper water depth at a rate 3×10^{-3}. (Bruce 1995; Krauss 1996).
5) *Amplitude.* Eddy currents near the sill have an amplitude of about 50 cm s^{-1} and a Rossby number $O(1)$. (Worthington 1969; Krauss 1996).
6) *Vertical structure.* Eddy currents observed near the sill have a nearly uniform phase with depth. (Smith 1976). Eddy currents have a maximum amplitude at a depth well above the maximum of the mean flow. (Dickson and Brown 1994; Krauss 1996).
7) *Water mass properties.* The eddies have a signature of Arctic Intermediate Water in their cores. (Cooper 1955; Bruce 1955; Krauss 1996).
8) *Vorticity.* The strongest eddies are cyclones. (Bruce 1995).
9) *Comparison to other overflows.* Mesoscale variability is considerably stronger in Denmark Strait than in other major overflows. Our assessment of historical observations.

midlevel cyclogenesis. Whether PV outflow is the underlying cause is not clear, and even if it were, the hypothesis does not indicate the form that the cyclonic relative vorticity will take (the observations show discrete cyclones). To test the PV outflow hypothesis directly we have chosen to employ numerical experiments in which the buoyancy forcing over the marginal sea is altered in order to achieve an outflow in one or more layers.

The numerical model used here is based on the Miami Isopycnal Coordinate Ocean Model (MICOM) documented by Bleck et al. (1992). This model solves the primitive equations for the isopycnal layer averaged quantities of horizontal momentum, layer thickness, temperature, and salinity using an isopycnal vertical coordinate.

a. Model equations

The horizontal momentum equation for a layer may be written as

$$\frac{\partial \mathbf{v}}{\partial t} + \boldsymbol{\nabla}\frac{\mathbf{v}^2}{2} + (\zeta + f)\mathbf{k} \times \mathbf{v} + \boldsymbol{\nabla} M = -g\alpha\frac{\Delta\tau}{h} + h^{-1}\boldsymbol{\nabla}\cdot(\nu h \boldsymbol{\nabla}\mathbf{v}), \quad (1)$$

where $\mathbf{v} = (u, v)$ is the horizontal velocity vector, $\boldsymbol{\nabla}$ is the along-isopycnal gradient, $\zeta = \partial v/\partial x - \partial u/\partial y$ is the relative vorticity, f is the usual Coriolis parameter, $\mathbf{k}$ is the vertical unit vector, $M = gz + p\alpha$ is the Montgomery potential, p is the hydrostatic pressure, α is the specific volume of the layer (constant), $h = \Delta p/\rho g$ is the thickness of the layer, ν is a variable eddy viscosity, and $\Delta\tau$ is the stress difference across the layer of thickness h. Pressure is computed from the hydrostatic relation and $p = 0$ at the free sea surface. The only vertical mixing process is the stress, τ, due to bottom drag, which is parameterized through a quadratic bulk formula as

$$\tau = c_D \rho_0 |\mathbf{v}|\mathbf{v}, \quad (2)$$

where c_D is a bottom drag coefficient. The bottom drag is applied uniformly over the thickness of the bottom layer, or 10 m, whichever is greater. The eddy viscosity ν is proportional to the total horizontal deformation (Smagorinsky 1963; Bleck et al. 1992) in the form

$$\nu = \eta[(u_x - v_y)^2 + (v_x + u_y)^2]^{1/2}\Delta x^2, \quad (3)$$

where $\Delta x = 2$ km is the grid spacing and $\eta = 0.1$ is a nondimensional factor. In regions of weak shear the eddy viscosity is less than 10 m^2 s^{-1}, while for very strong shears [Rossby numbers $O(1)$] it can be as large as 40 m^2 s^{-1}. The Coriolis parameter $f = 10^{-4}$ s^{-1} throughout the model domain.

The lateral boundary conditions are no-slip for momentum and no-flux for density. The no-slip boundary conditions are also partially implemented in the interior for the bottom layer in regions of a sloping bottom. The intent here is to gradually transition the frictional parameterization from bottom drag only for the case of a flat bottom to no-slip for the case of very steep topography. The velocity shear used to calculate the lateral momentum flux in the parameterization of subgrid-scale mixing between points j and $j - 1$ (for example) is calculated as

$$\frac{\partial u}{\partial y}\Delta y = [u_j - (1 - \kappa)u_{j-1} + \kappa u_j], \quad (4)$$

where the aspect ratio $\kappa = \Delta H/h$ $(0 \le \kappa \le 1)$, ΔH is the change in depth between adjacent grid points, h is the layer thickness, Δy is the grid spacing between points j and $j - 1$. If the topography is sufficiently steep that it changes depth by an amount equal to or greater than the layer thickness, then the lateral boundary condition is treated as a no-slip side boundary. If the bottom topography is flat there is no additional friction applied. The details of this treatment (Bleck and Smith 1990) are not important to the qualitative behavior of the model, but this approach does make the bottom layer more viscous than for calculations with bottom drag (2) only.

The continuity equation is represented as a prognostic equation for the layer thickness h,

$$\frac{\partial h}{\partial t} + \nabla \cdot (\mathbf{v}h) + \delta w_i = \nu_h \nabla^2 h, \tag{5}$$

where $\nu_h = 20$ m^2 s^{-1} and constant. The variable w_i represents a cross-isopycnal mass flux and is used to parameterize buoyancy forcing (more on this in section 2c). Diapycnal fluxes are otherwise zero. There is no surface heating or freshwater flux so that temperature and salinity need not be discussed.

b. Model configuration

The model is configured in a closed domain that measures 720 km by 100 km and includes two basins separated by a sill (see Fig. 4). Although the model is configured on an f plane, the shallow basin will be referred to as the high latitude, or northern, basin and the deep basin is the low latitude, or southern, basin. The northern basin is 1500 m deep, the southern basin is 3000 m deep, and the sill depth is nominally 1000 m. The topography slopes uniformly downward toward the interior of the northern basin from the western, eastern, and southern directions, with the slope from the sill being fairly weak (0.002). The topography of the southern basin slopes uniformly down from the sill at the north (slope of 0.03) and from the western boundary (nominal slope of 0.02). This idealized configuration allows us to investigate the topographic influence on an overflow by varying a small number of parameters, principally the sill depth and the western boundary slope that underlies the overflow south of the sill (experiments described in section 5).

c. Initial condition and buoyancy forcing

The vertical stratification is represented by three layers of density $\rho_1 < \rho_2 < \rho_3$ (Fig. 4b). In the northern basin, which is regarded as the marginal sea, the initial stratification has water of density ρ_1 down to a depth of d_1, water of density ρ_2 down to the depth of the sill, and the deep northern basin is filled with water of density ρ_3. In the southern basin, the uppermost layer initially extends down to a depth d_1 and the second layer extends from d_1 down to the bottom. Thus, the initial state has no water of density ρ_3 in the southern basin.

The model is forced by a diapycnal mass flux from layer 1 into layers 2 and 3 at specified rates over the shaded region in Fig. 4a, as indicated schematically by the downward arrows in Fig. 4b. The diapycnal mass flux in the remainder of the basin is set to zero. The model equations can include turbulent entrainment, and we expect that there are regions of intense diapycnal mixing in the real oceanic overflows (e.g., Price and Baringer 1994). This process is nevertheless omitted to simplify the physics and the interpretation.

For most calculations, water of density ρ_2 and ρ_3 is formed over the northern basin at a constant rate, 1.5×10^6 m^3 s^{-1}. This water comes from the upper layer so that the stratification changes slowly toward more dense waters and less surface water. Over the duration of the calculations reported here (100 days), the average depth of layer 1 in the southern basin decreases by about 15% of its initial thickness. Eddy statistics are nevertheless stationary toward the end of the present integrations, and some calculations that included a compensating region of warming near the southern boundary have shown no major differences from those reported here. Hence we believe that the slow drift of the stratification is not significant.

The goal here is to investigate the impact of having mid and lower outflow layers (as occurs in Denmark Strait) and to contrast this to the case of a single overflow layer (Faroe Bank Channel and the Strait of Gibraltar). Our only means of controlling the structure of the outflow is by imposing an internal buoyancy flux over the northern end of the marginal sea. This very indirect method has the advantage (we think) that the flow itself determines its approach to the sill and its structure (PV gradients, etc.) as it enters the open ocean. An attendant consequence is that the outflow transport is not directly specified; we typically find that southward transport at the sill is only about 20%–40% of the deep-water formation rate. Thus, more than half of the newly formed deep and midlevel water simply accumulates in the northern basin during the time of these integrations.

d. A few cautionary remarks

In what follows we indentify layer 3 with the Denmark Strait overflow and the midlevel outflow (layer 2) with the Arctic Intermediate Water. Other semiquantitative comparisons with Denmark Strait observations are also made. It should be emphasized, however, that these numerical integrations are better regarded as process studies intended to make a qualitative test of the PV outflow hypothesis rather than as detailed simulations of the full circulation through Denmark Strait. In particular, the model configuration (Fig. 4) has sacrificed realistic basin topography and vertical resolution for the sake of very high horizontal resolution, which seemed essential to resolve mesoscale variability, and for conceptual simplicity. A consequence is that we cannot achieve realistic wind forcing in such a small basin, and thereby forfeit the prospect of having a realistic upper-layer circulation (analogous to the southward flowing East Greenland Current). In a few experiments we generated an outflowing upper layer by applying a massive cyclonic stress curl. The eddy formation process described in detail in the next few sections was not strongly affected by the wind-forced circulation, but two features that could be important in a different context, the eddy translation speed and the net outflow transport, *are* affected by the wind-forced circulation and are not reproduced well in the present simulations. In a similar way, we have run integrations with five layers and find that the main conclusions hold.

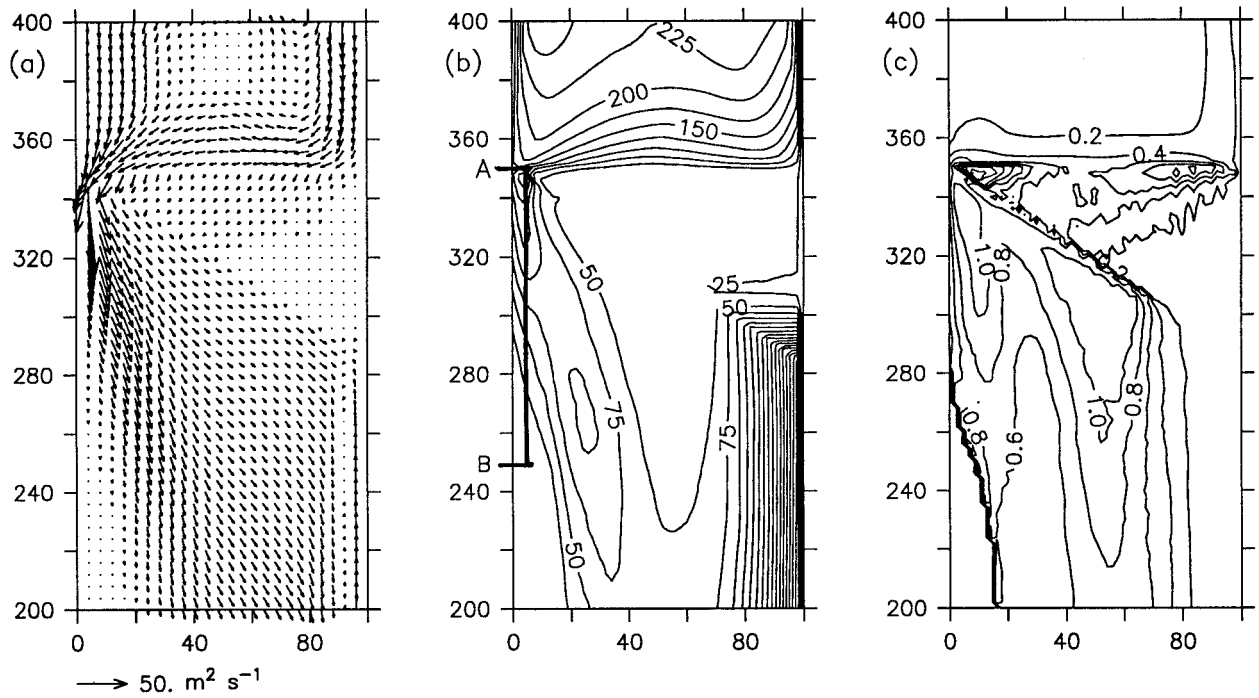

FIG. 5. Mean fields for the dense overflow layer in the vicinity of the sill: (a) transport vectors (every other point), (b) layer thickness (m), and (c) Froude number $F = \mathbf{v}/(g'h)^{1/2}$. The sill is located at 350-km latitude, the marginal sea is at the top of the figure.

3. Simulation of a two-layer outflow

The central case described in this section was initialized with an upper-layer thickness $d_1 = 1000$ m, a sill depth of 1000 m, the topographic slope along the western boundary $\alpha = 0.02$, a density difference $\rho_3 - \rho_2 = 0.1$ kg m^{-3}, and other parameters as given in the previous section. The model was integrated for 100 days and statistics were calculated over the final 60 days, which appeared to be stationary. This analysis emphasizes the region just downstream of the sill where the overflow waters adjust to the stratification of the southern basin and begin their descent along the sloping bottom.

a. Mean fields

1) THE OVERFLOW LAYER

The mean velocity, layer thickness, and Froude number [$F = \mathbf{v}(g'h)^{-1/2}$, where $g' = g(\rho_3 - \rho_2)/\rho_0$ is the reduced gravity and h is the thickness of layer 3] of the dense overflow (layer 3) are shown in Fig. 5 for the sill and downstream region (the sill is located at 350-km latitude).

Much of the lower-layer water that overflows the sill approaches the sill along the eastern side of the strait (Fig. 5a), even though its source region is over the topography in the northwest corner. This eastern boundary current results from the compression supplied to the lower-layer water as it approaches the sill from the north and feels the shoaling bottom topography (see Fig. 4b). In an attempt to conserve potential vorticity, the lower-layer current develops anticyclonic vorticity, which drives the current toward the eastern boundary. [A similar approach along the eastern side of the strait is found just north of the real Denmark Strait, as indicated in the hydrographic and current meter section described by Smith (1976), and in the atlas of Ross (1982).] As the sill is finally reached, the lower-layer current turns sharply to the west approximately following contours of constant depth until the western boundary is reached. It then turns to the south and overflows the sill along the western boundary.

The region extending approximately 50 km downstream of the sill is supercritical for the deepest layer, as indicated by the Froude number being greater than 1 in Fig. 5c. This transition to supercritical flow occurs very rapidly; the maximum mean velocity is only 29 cm s^{-1} just 2 km upstream of the sill, increases to 60 cm s^{-1} at the sill crest, and then decreases to 48 cm s^{-1} at just 2 km downstream of the sill. Coincident with this rapid acceleration there are also rapid changes in the mean layer thickness. Although we believe that very rapid transitions near the sill are to be expected, these sharp gradients are not well resolved in the present grid, which has 2-km spacing, and thus most of our description will be on the region of weaker gradients within 150 km downstream of the sill itself. This is also the region in which mesoscale variability is most pronounced.

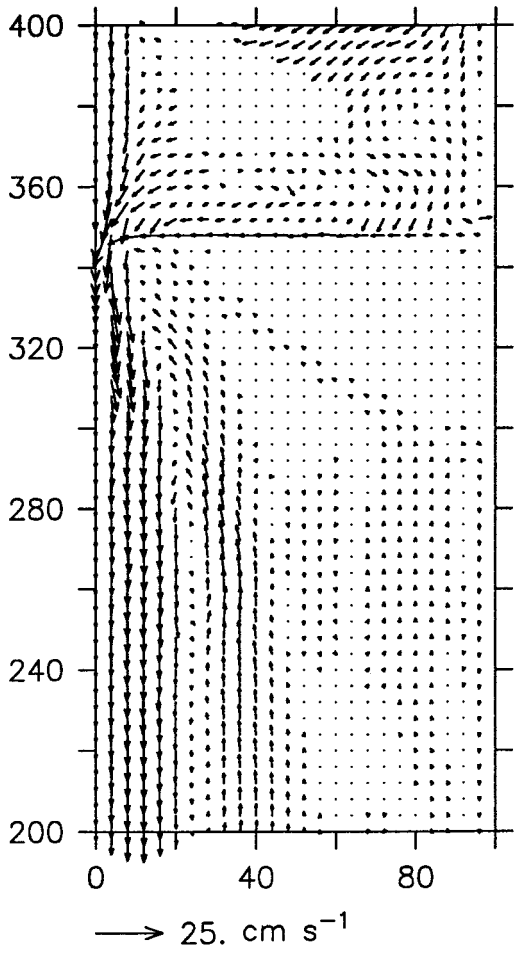

FIG. 6. The mean velocity in the upper overflow layer (every other point).

The mean path of the overflow layer downstream of the sill is evident in both the transport and layer thickness fields. The overflow layer descends the western slope at an angle of about 15° near the core, and at a somewhat steeper angle on the offshore side where the overflow layer is quite thin (thickness of 20–30 m) and very strongly effected by bottom friction. This sort of viscous-induced draining of a density current has been described in laboratory experiments by Smith (1977) and by Lane-Serff and Baines (1998, hereafter LSB). The pressure gradient in the alongslope direction that is set up by the descent of the overflow layer is important to the coupling between the midlevel and overflow layers, as will be discussed further in section 4. The deep basin is slowly filled with this dense water, as can be seen by marked increase in layer thickness toward the eastern boundary.

2) MIDLEVEL OUTFLOW LAYER

The approach of the outflow water is primarily along the western boundary (Fig. 6), although some water approaches along the eastern boundary and then flows to the west along the sill crest as described above for the overflow layer. This difference in approach to the sill arises because the midlayer is largely shielded from the compression effects of the bottom topography by the presence of the deeper overflow layer. Calculations with additional layers show that only the deepest layer approaches the sill from the east, all others remain primarily along the western boundary. There is an acceleration of the midlevel outflow as it passes over the sill, but the flow remains subcritical (maximum Froude number is approximately 0.6) mainly because the thickness of this layer increases as soon as the water flows into the southern basin (recall that the southern basin is initially filled with water of this density). This change in the thickness of this layer is an example of midlevel stretching, and has important consequences for cyclogenesis, discussed next. Downstream of the sill, the mean current in the midlayer is toward the south along the western boundary current, and there is a weaker, northward flowing countercurrent just offshore.

b. Eddy variability

Both layers are highly time dependent just downstream of the sill (Fig. 7). There are two regions of enhanced variability, one small area located right at the sill crest (350-km latitude), and another larger area that extends approximately 150 km downstream of the sill. Again, we will focus on the downstream region because we believe that it is better resolved by the numerical model and is the region most relevant to the eddy formation process. The eddy kinetic energy is considerably larger in the midlevel outflow layer (maximum of approximately 175 cm^2 s^{-2}) than it is in the deep overflow layer (maximum of approximately 100 cm^2 s^{-2}), although the spatial extent of the region of high variability is similar in the two layers.

1) MIDLEVEL OUTFLOW LAYER

An instantaneous view of the velocity field indicates the structure of the mesoscale eddies that give rise to this variability. Figures 8a and 8b show the velocity and potential vorticity field in the midlevel on day 57. The region of high eddy kinetic energy is populated with four strong cyclonic eddies that are approximately 20–30 km in diameter. These eddies move generally southward, but with a definite tendency to move out to deeper water. The rate, $\partial H/\partial s \approx 4 \times 10^{-3}$, is similar to that observed in the real Denmark Strait cyclones by Bruce (1995). In the numerical model, the eddies follow a path above the onshore side of the core of the overflow layer (an explanation of this is in section 4). The maximum velocity in these eddies is about 60 cm s^{-1} so that peak Rossby numbers are greater than 1.

These eddies are characterized by high potential vorticity, which can be traced back upstream into the mar-

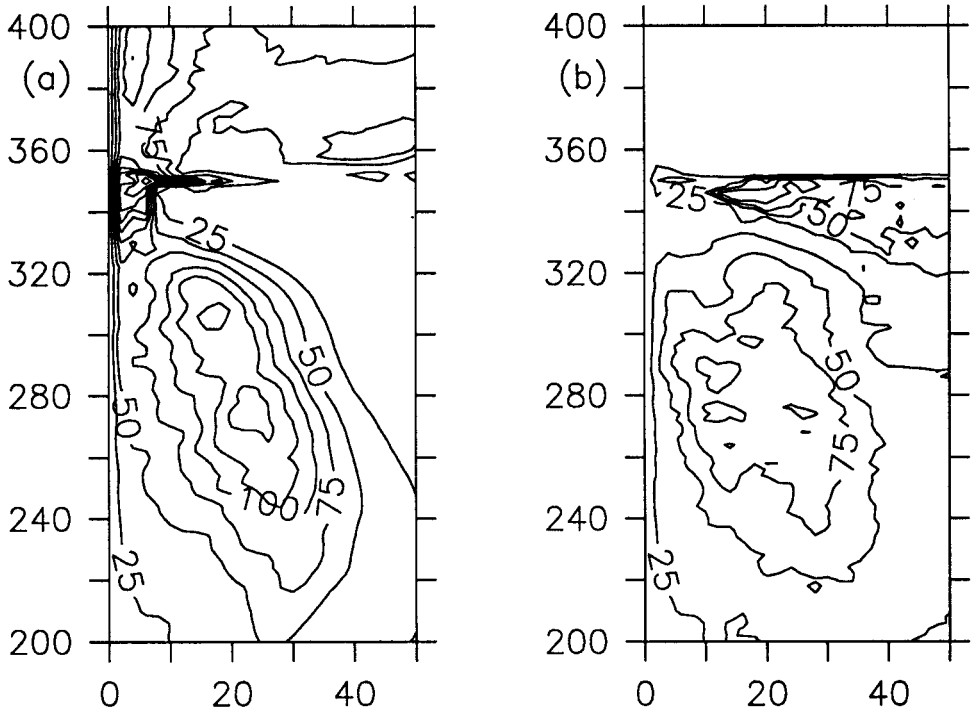

FIG. 7. Eddy kinetic energy for (a) midlevel outflow (layer 2) and (b) dense overflow (layer 3) ($cm^2\ s^{-2}$). Only the western 50 km of the model domain is shown.

ginal sea. The no-slip lateral boundary conditions give rise to a narrow region of large negative potential vorticities so that there is a change in sign of the cross-stream potential vorticity gradient in the outflow layer. However, because free-slip boundary conditions do not produce a region of large negative potential vorticities along the boundary, yet still form cyclones much in the same way as the no-slip calculation, we feel that the change in sign of the potential vorticity gradient near the sill is not an essential component of the eddy formation process. The higher stratification in the core of the eddies is evident in the layer thickness field (Fig. 8d, which is similar to potential vorticity, though the latter is a more useful indicator of origin). The high potential vorticity in the core of these eddies is eroded by lateral subgrid-scale mixing as the eddies propagate downstream.

These cyclonic eddies strongly dominate the transport in the mid layer, as shown in Fig. 8c. Time averaging of this field nevertheless produces a mean southward western boundary current, and a northward countercurrent on the offshore side of the mean path of the eddies. Time averaging obscures the fact that most of the transport in the midlevel is carried southward in the form of discrete eddies.

2) OVERFLOW LAYER

The main core of the overflow layer shows a meandering pattern on the same horizontal scale as the midlevel eddies (Figs. 9a–d). The potential vorticity and layer thickness fields indicate that much of the transport in the overflow layer is carried in a series of domes or boluses approximately 150–200 m thick and 30 km in diameter superimposed on a larger-scale bottom current. These boluses of overflow water are directly beneath the midlevel cyclones, and they too have a cyclonic circulation (although the vertical shear in velocity is anticyclonic, as expected for a dense bolus of bottom water). Maximum velocities in the deep layer are about 40 cm s^{-1}, or slightly less than in the midlevel. The potential vorticity increases monotonically from the western boundary into the interior just downstream of the sill.

The cyclonic nature of the circulation in the deep eddies indicates that they are formed by an upward motion of the interface between layers 2 and 3, consistent with the expected response to the introduction of a high potential vorticity anomaly in the layer above. No such perturbations are found in the absence of a high potential vorticity source in the midlevel outflow layer (experiments described in the next section); hence we conclude that the eddies seen in the overflow layer are driven by an adjustment process in the midlevel outflow layer. This scenario is quite different from that found in the baroclinic instability models of Smith (1976), Swaters (1991), and the interpretation of eddy formation in the numerical calculations of Jiang and Garwood (1996).

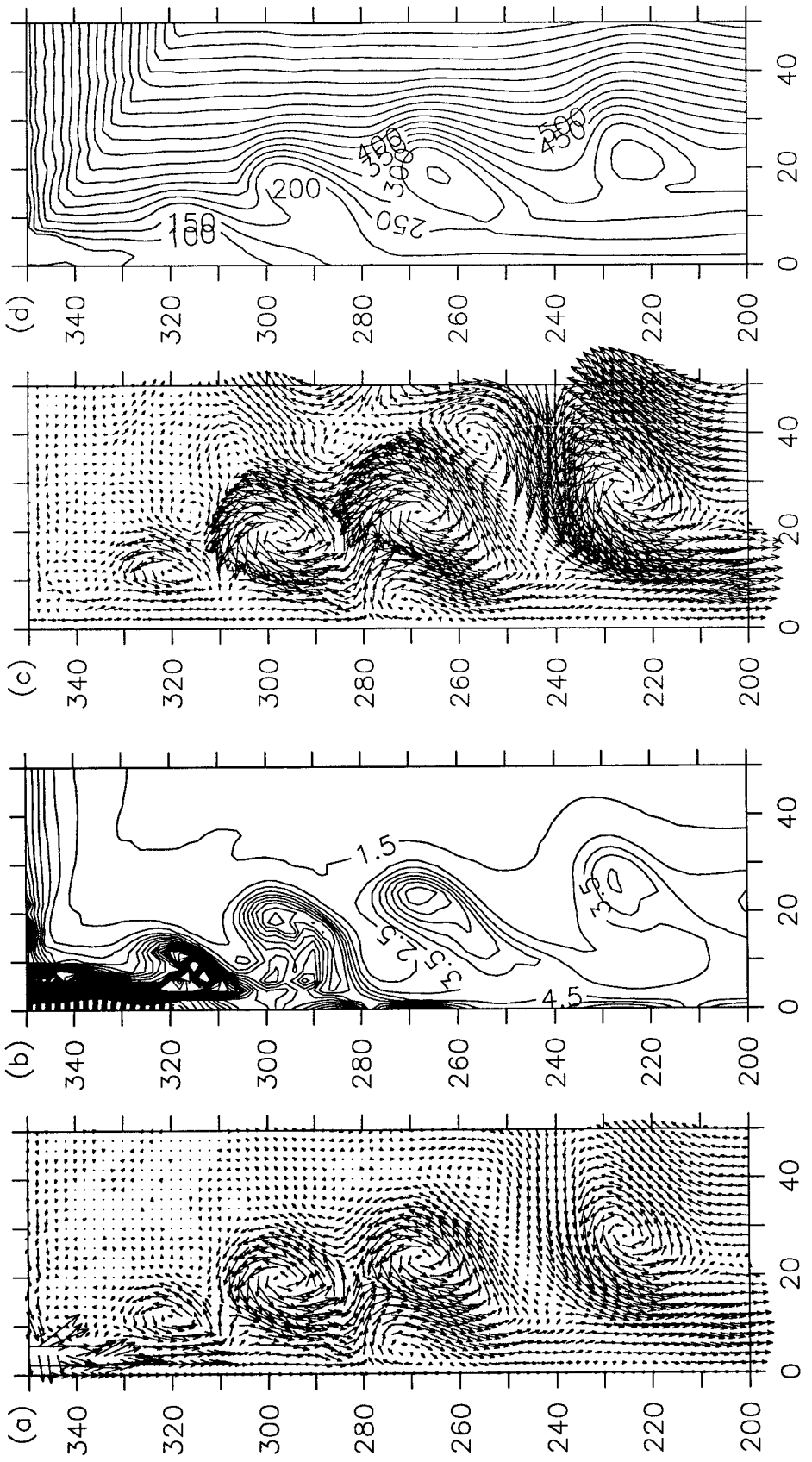

FIG. 8. Layer 2 model fields on day 57 for the central case (a) velocity, (b) potential vorticity (10^{-7} m^{-1} s^{-1}), (c) transport vectors, and (d) thickness (m).

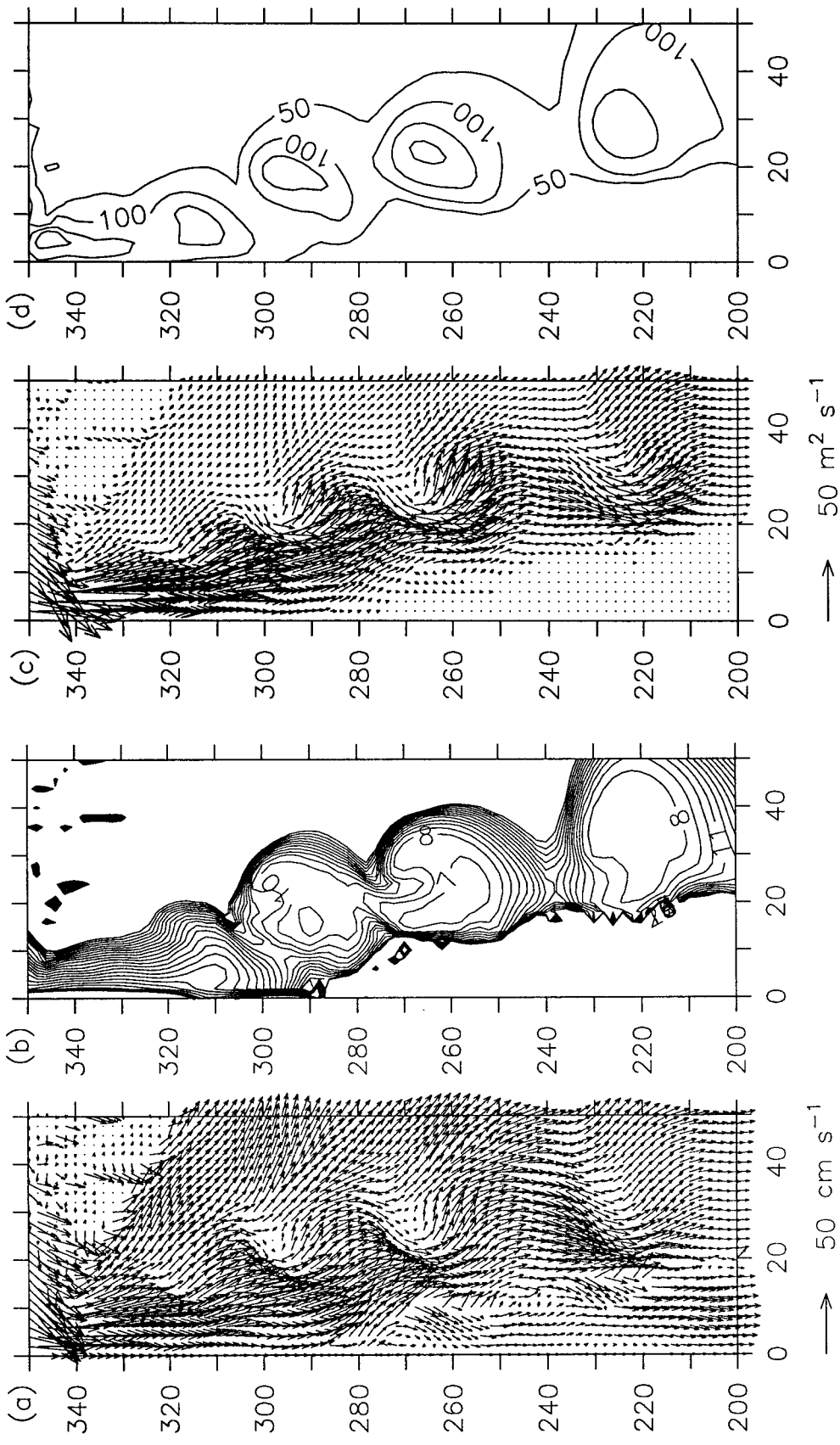

FIG. 9. Layer 3 model fields on day 57 for the central case (a) velocity, (b) potential vorticity (10^{-7} m^{-1} s^{-1}), (c) transport vectors, and (d) thickness (m).

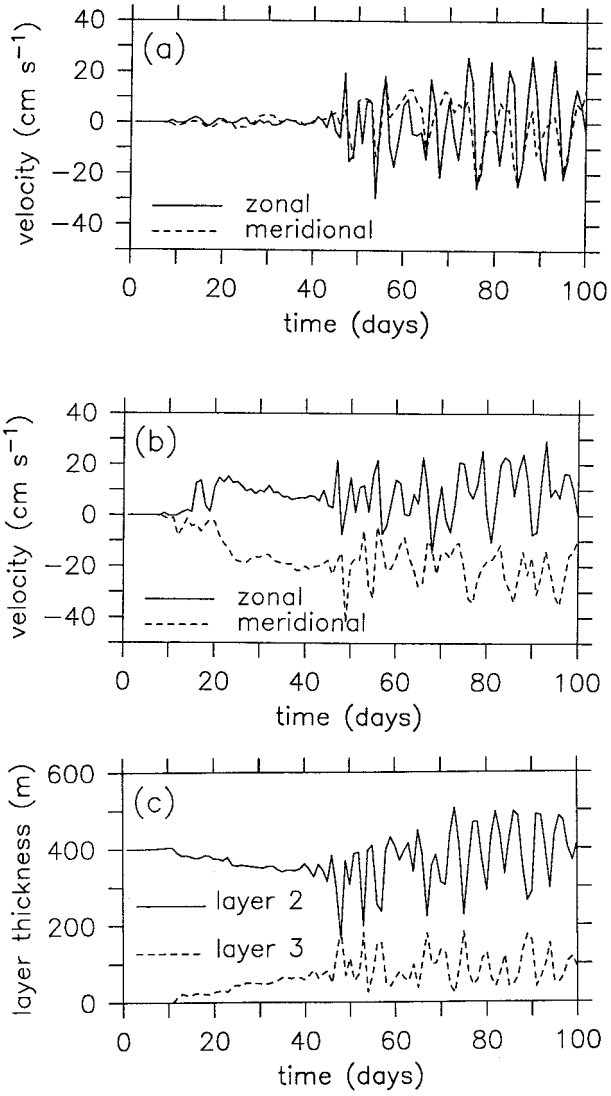

FIG. 10. Time series of horizontal velocity for (a) layer 2 and (b) layer 3, and (c) thickness for both layers 2 and 3 at a location 50 km downstream of the sill (latitude 300 km, longitude 20 km).

3) EDDY TIMESCALE AND THE ONSET OF CYCLOGENESIS

The onset of cyclogenesis and the frequency of these eddies can best be seen in a time series of the velocity and thickness taken just downstream of the sill (300 km latitude, 20 km longitude) shown in Fig. 10. Deep-water formation is started at day zero, and by day 20 the deep layer has begun to overflow at full strength. There is, however, very little eddy activity until day 40, at which point the midlevel outflow also begins to flow southward across the sill (not clearly evident in the midlevel velocity at the point observed in Fig. 10). From then on, cyclonic eddies are spawned about every 4 days and are clearly evident in both layers. This sudden onset of cyclogenesis around day 40 suggests that a coupling between the two outflowing layers is an essential ingredient of the cyclogenesis process, an important point that we will develop further in section 4.

There is also some lower level of eddy variability within the marginal sea, and more at the sill crest. There is no obvious 4-day periodicity, however, suggesting that this timescale is intrinsic to the flow regime downstream of the sill.

The maximum velocity in the eddies at this site is about 30 cm s^{-1} with layer thickness anomalies of 200 m in both the midlevel and overflow layers. The passage of cyclones (and thin layers) in the midlevel coincides with cyclones (and thick layers) in the overflow layer. Thus, the variability of vorticity (layer thickness) is almost exactly in (out of) phase between the mid and overflow layers (Fig. 10c).

This eddy variability has many of the characteristics of the mesoscale variability observed in Denmark Strait [reviewed in section 1b(2) and Table 1 and discussed further below), although the quantitative behavior (particularly the eddy period, which is somewhat longer here than is observed in Denmark Strait) is sensitive to the choice of geophysical parameters as described in detail in section 5.

4. Cyclogenesis in outflows and overflows

a. A test of the PV outflow hypothesis

To make a direct test of the PV outflow hypothesis we can simply shut off the diapycnal volume flux (deep-water formation) into one or the other of the layers.

Outflow only. If the central case is repeated with a flux of 1.5×10^6 m^3 s^{-1} into the midlevel, but with no production of overflow water, then the midlevel begins to outflow by about day 20, as before. But quite unlike the central case, the flow south of the sill is nearly steady (a snapshot of the velocity on day 55 is shown in Fig. 11). No cyclones are formed in the midlevel, and neither is there significant variability in the deep overflow layer.

Overflow only. If the central case is repeated with a flux of 1.5×10^6 m^3 s^{-1} into the deep overflow layer, but with no production of midlevel water, then there are some cyclonic eddies in the midlevel, but they are much weaker than in the central case and are formed later in the integration. An example of these eddies on model day 80 is shown in Fig. 12. The eddy kinetic energy in the overflow layer averaged over the region 150 km downstream of the sill is about 12% of the average eddy kinetic energy in the central calculation where there were two outflowing layers.

The evidence above is that cyclogenesis is considerably stronger and more sustained in simulations in which there are two outflowing layers (and a potential vorticity anomaly in the midlevel layer). The PV outflow hypothesis is broadly consistent with this result in that it predicts a correlation of phenomenon that we do observe. However, it is also clear that cyclogenesis can

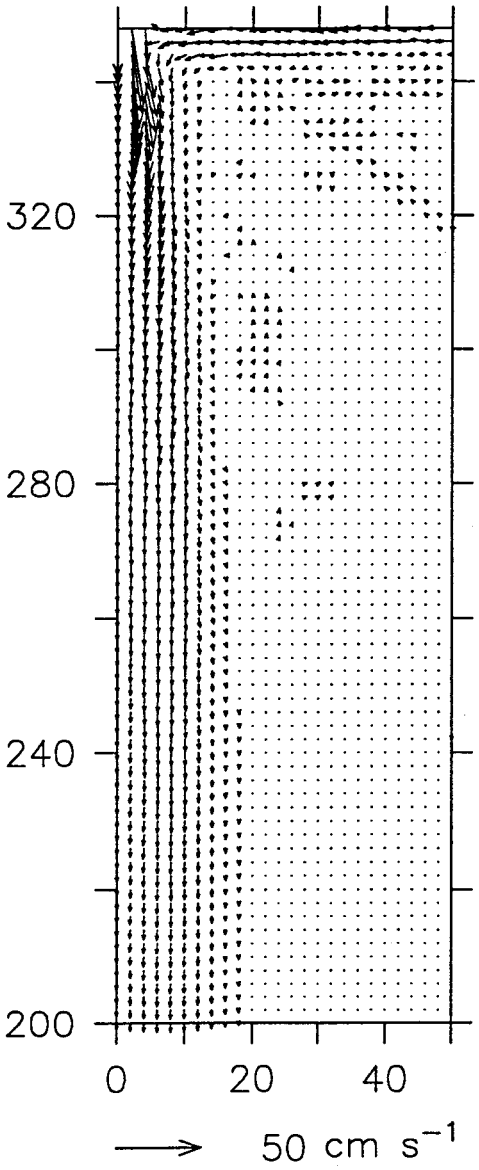

FIG. 11. Velocity field for layer 2 on day 55 for the case with no dense overflow water formed north of the sill. The midlayer flow remains along the western boundary and no strong cyclones are formed.

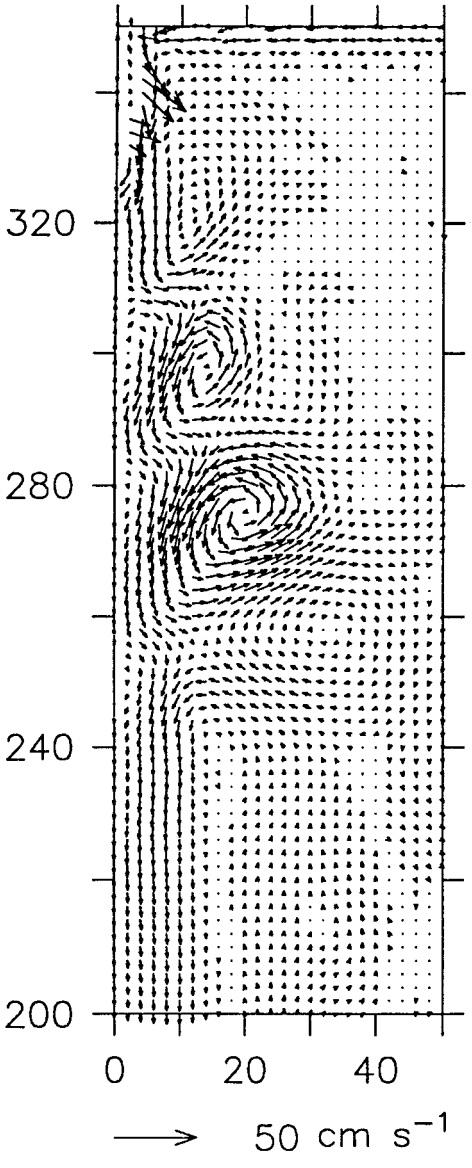

FIG. 12. Velocity field for layer 2 on day 80 for the case with no water formed in the midlayer north of the sill. Some cyclones are formed but they are weaker and are formed later than for the central case.

occur under conditions that are not subsumed under the PV outflow hypothesis. Thus, the PV outflow hypothesis indicates sufficient but not necessary conditions for cyclogenesis. To approach the latter we have to understand more of the mechanism(s) of cyclogenesis.

b. The mechanics of cyclogenesis

We interpret the cyclogenesis described above to be the result of the introduction of a potential vorticity anomaly into the open ocean. There appear to be two essential ingredients required for the sustained production of strong midlevel cyclones in this manner: 1) There has to be a potential vorticity gradient in the layer above the dense overflow and, assuming that the cyclogenesis is sustained, then there has to be some source for this potential vorticity anomaly. 2) There also has to be a mechanism to move this potential vorticity anomaly offshore so that stretching can occur. We take up the latter step first.

1) COUPLING BETWEEN THE OUTFLOW LAYERS

Offshore advection in the midlevel occurs in these simulations by a simple, although perhaps not obvious, coupling between the deep and midlevel layers through

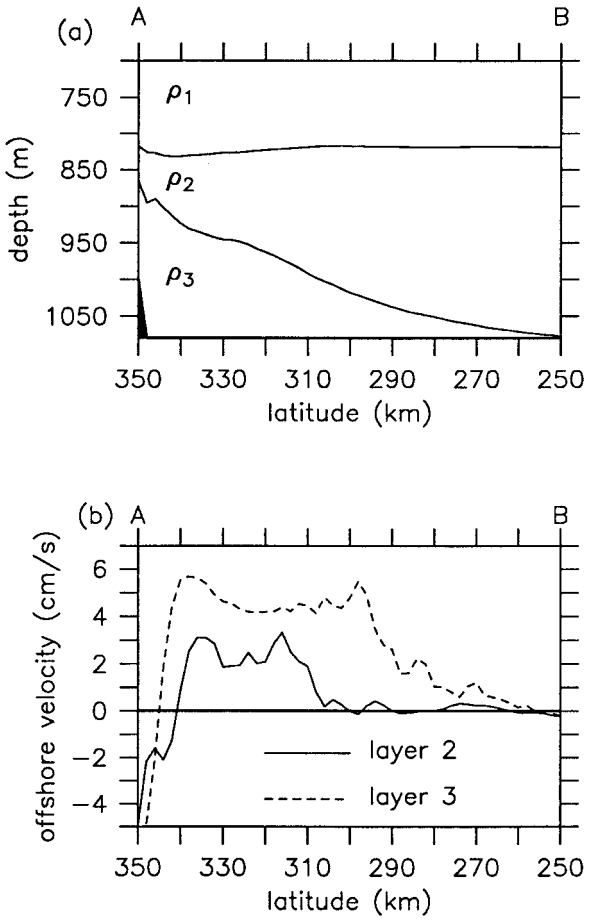

FIG. 13. North–south section along line A–B in Fig. 5: (a) layer interface depths and (b) offshore velocity.

the thermal wind relation. As the deep overflow layer descends the slope downstream of the sill (due to bottom friction), the interface of the onshore side of the deep overflow deepens to the south. This is shown in Fig. 13a by the mean depth of the layer interfaces along a north–south section 4 km off the western boundary (its position is indicated as section A–B in Fig. 5). The thickness of layer 3 decreases from approximately 150 m near the sill to zero at about 100 km downstream of the sill. This sloping isopycnal gives rise to an alongslope pressure gradient balanced by a vertical shear in the offshore geostrophic velocity between the deep overflow and the midlevel layer above. (By offshore velocity, we refer to the zonal velocity and not the velocity component perpendicular to the path of the dense overflow.) The sense of this shear is to transport water in the midlevel away from the boundary and toward deeper water. The mean offshore velocity along this section is about 2 cm s^{-1} (Fig. 13b), in general agreement with the thermal wind of the sloping interface. If there exists an offshore potential vorticity gradient in the midlevel layer above the deep overflow, say with high potential vorticity on the onshore side of the outflow, then the geostrophic shear will advect this high potential vorticity water out toward the core of the deep overflow. Because of the reversal in shear on the offshore side of the overflow, these midlevel anomalies are then trapped above the onshore side of the core of the deep overflow.

As the high potential vorticity water is advected into the low potential vorticity interior it develops cyclonic vorticity in accordance with the gradient wind balance. The thickness of the parcel also increases along with the relative vorticity in an attempt to conserve potential vorticity. This interplay between relative vorticity generation through gradient wind balance and stretching (which feeds back on the lateral pressure gradients) continues until a balanced vortex exists (McWilliams 1988). Vortex spinup occurs on the inertial timescale, consistent with the emergence of fully developed large amplitude vortices within an eddy diameter downstream of the sill. Once at large amplitude, the eddies feel the topographic slope and propagate to the south at the topographic Rossby wave phase speed, which for short waves is independent of the diameter of the eddies. Propagation away from the source region concludes the formation of a single cyclonic eddy, and the continuing outflow begins the adjustment process anew. High potential vorticity water of the midlevel outflow is thereby transported to the south (shallow water on the right) in a series of discrete cyclones.

An important effect of the bottom topography is thus to provide a propagation mechanism for the midlevel outflow water. Model experiments show that, if the bottom is made flat so that the propagation speed of the eddies goes to zero, then only a single cyclonic eddy is formed downstream of the sill. This eddy does not propagate southward and, instead, remains nearly stationary as it grows by the steady accumulation of outflow water.

The importance of the alongslope pressure gradient induced by the descent of the overflow layer is revealed by a series of calculations in which the strength of the bottom drag is varied. Increases in the bottom drag above that used in the central case result in a more rapid descent of the dense current down the topographic slope, a stronger alongslope pressure gradient, and a more rapid formation of cyclonic eddies in the midlevel. A calculation with vanishing bottom drag and vanishing sidewall friction on the interior points results in similar cyclonic eddies, but they do not attain their full strength until much farther downstream of the sill (approximately 130 km downstream compared to 30 km for the central case). The overflow still broadens slowly downstream of the sill even with vanishing bottom drag because of along-isopycnal frictional parameterizations in the continuity and momentum equations. (Purely inviscid calculations are not possible due to numerical stability requirements.) This slow spreading of the overflow layer once again gives rise to an alongslope pressure gradient and an offshore geostrophic flow in the midlevel that couples the midlevel to the overflow current. However, the location at which the midlevel cyclones form is di-

rectly dependent upon the strength of the alongslope pressure gradient in a way that is consistent with the coupling mechanism described above.

The role of the deep overflow is now made clear, the geostrophic shear that arises as a result of the alongslope pressure gradient provides a mechanism to advect the high potential vorticity water off the boundary and into the interior where it then adjusts and develops into cyclones.

2) SOURCES OF HIGH POTENTIAL VORTICITY

For the present model configuration, there are two sources of the high potential vorticity water required to make cyclonic eddies. The midlevel outflow water is more strongly stratified than is the water of this density class in the southern basin. The southward transport of this water in the outflow provides a continuous supply of high potential vorticity water along the boundary south of the sill (the PV outflow hypothesis). We believe this is analogous to the outflow of Arctic Intermediate Water through Denmark Strait (Figs. 2 and 3).

There is a second source of high potential vorticity water that is probably very important in laboratory and some other numerical experiments (details in section 6). The decreasing thickness of the midlevel layer over the sloping bottom gives rise to a region of high potential vorticity in the initial condition that is not due to the outflow per se. The weak cyclones that are formed in the midlevel in the absence of a midlevel outflow (Fig. 12) are a result of the geostrophic advection of this water offshore. We believe that this is the source of the midlevel cyclones in the calculations of Jiang and Garwood (1996). This source is very different from the outflow source, however, as the addition of stratification in the southern basin will greatly reduce the volume of high potential vorticity in the initial state and, thereby, suppress the generation of cyclonic vortices drawn from this water.

This influence of the different sources of high potential vorticity in the midlevel is further demonstrated by a series of calculations in which the potential vorticity gradient resulting from the bottom topography is varied. The maximum potential vorticity initially found in the southern basin is greatly reduced when the depth of the topography along the western wall is increased from 1000 to 1500 m, while still keeping the interface depth d_1 and the sill depth at 1000 m, and the bottom slope at 0.02. The case with outflow in both layers produces cyclonic eddies that are quite similar in structure to those in the central case (an example is shown in Fig. 14a), although the amplitude is slightly less, the diameter is larger, and the frequency is a little lower. The case with no midlevel outflow is now eddy-free, as indicated by the velocity field in Fig. 14b. The disappearance of the weak cyclones found in the previous single layer overflow case (Fig. 12) confirms that their source was the high potential vorticity present along the western boundary as part of the initial condition. Similar dependence upon the presence of a midlevel outflow is found if the interface between layer 1 and layer 2 is initialized above the sill depth with the same topography as in the central case, thus reducing the maximum potential vorticity initialized in the intermediate layer south of the sill.

These results confirm that the formation of cyclones requires a potential vorticity gradient (high potential vorticity near the boundary for cyclonic eddies) over a descending plume. This gradient can be supplied by a continuous outflow of high PV water (as is the case for Denmark Strait), or it may be present in the initial state of the southern basin as a result of weak stratification and a sloping bottom (relevent in laboratory and some numerical experiments).

5. Parameter dependence

The cyclogenesis process discussed in the previous sections is found for a fairly wide range of geophysical parameters (bottom slope, stratification, etc.) including those analogous to Denmark Strait, and for model parameters (slip or no slip boundary conditions, bottom drag). The amplitude and size of the cyclones does depend upon the geophysical parameters in a fairly straightforward way, as we will describe in this section. An understanding of parameter dependence helps to clarify the processes responsible for the cyclogenesis, and it may also help identify other regions in the ocean or atmosphere where similar phenomenon may occur.

a. Some effects of topographic slope

The frequency, horizontal scale, and energy of the cyclonic eddies found in the midlevel outflow just downstream of the sill are quite sensitive to the bottom slope along the western boundary. Figure 15 summarizes this dependency for calculations in which the bottom slope is increased from 0.005 to 0.04 while all other parameters are held fixed. The frequency and period of eddy formation ($\omega = 2\pi/P$, where P is the period and ω is the frequency) are shown in Figs. 15a,b as a function of the bottom slope. For the weakest slope, the eddies are formed about once every 8 days, while for the strongest slope the eddies are formed about once every 2 days. The formation frequency increases nearly linearly with the bottom slope in a way that is strongly reminiscent of the short topographic Rossby wave dispersion relation, $\omega = -\alpha N$, where $N = 10^{-3}$ s^{-1} (calculated from $g' = 10^{-3}$ m s^{-2} and $h = 1000$ m and which is also plotted in Figs. 15a,b). Thus the cyclones appear to propagate along the western slope as topographic Rossby waves. In this important respect, these cyclones are consistent with the instability waves that arise in the analytic model of a dense bottom current by Swaters (1991) and the linear baroclinic instability model of Smith (1976). Other characteristics of these

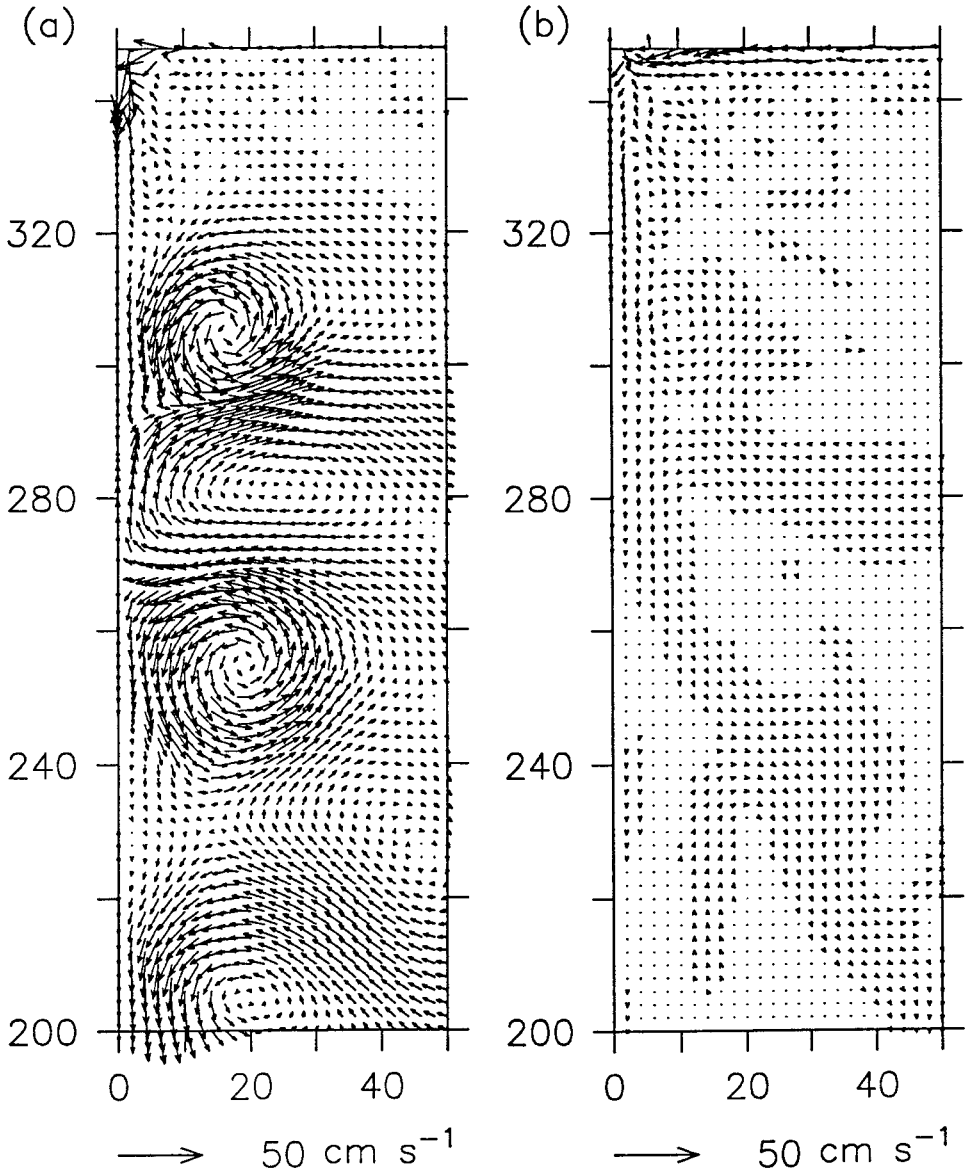

FIG. 14. Velocity field for layer 2 on day 55 for cases where the bottom topography intersects the western boundary at 1500-m depth, 500 m below the sill depth with (a) 1.5×10^6 m^3 s^{-1} formed in layer 2 and (b) no water formed in layer 2.

cyclones are very different from the unstable waves that are predicted by these theories.

The horizontal scale of the cyclones also varies as a function of the bottom slope, as indicated in Fig. 15c (note that the eddies for the weakest bottom slope of 0.005 are elliptical, not circular; the radius plotted is the average of the major and minor ellipse axis). The eddy diameter decreases with increasing bottom slope, and varies from a maximum of about 55 km to a minimum of approximately 20 km over this range of slopes. The internal deformation radius calculated for the two outflow layers is O(5–10 km) in all of these cases. The outflow transport is also nearly constant. This length scale dependency differs from that expected by the baroclinic instability models of Smith (1976), which predicts little dependency of the length scale on bottom slope, and Swaters (1991), which predicts increasing length scales with increasing bottom slope. The topographic Rossby wave dispersion relation provides no constraint on the length scale of the eddies in the short wavelength regime found here.

The horizontal scale of the eddies appears to be determined by their formation frequency, as noted above, and by a volume transport constraint that arises because these eddies carry nearly the entire transport of the mid-level outflow. If the frequency of eddy formation is

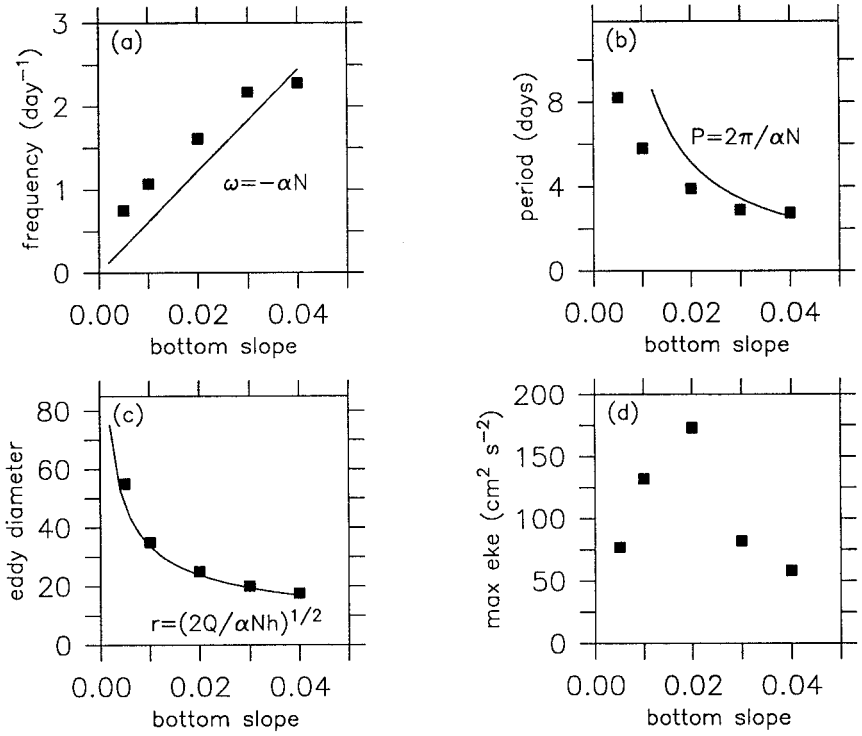

FIG. 15. Eddy characteristics as a function of bottom slope along the western boundary: (a) frequency of eddy formation and (b) period of eddy formation (the solid lines indicate the short topographic Rossby wave dispersion relation); (c) eddy diameter, the solid line is the diameter predicted by relation (7); and (d) maximum eddy kinetic energy.

caused to increase, due say to an increased bottom slope south of the sill that does not effect the outflow transport, then the eddy radius r must decrease so that the transport carried by the eddies remains constant; that is,

$$r = \left(\frac{Q_2 P}{\pi h}\right)^{1/2}, \tag{6}$$

where P is the time period between eddy formations, h is a representative thickness of the midlevel outflow density layer for the eddies (the eddies have a strong velocity signature over the entire depth of the water column, which is generally much greater than the thickness of the outflow layer only), and Q_2 is the total transport flowing over the sill in layer 2. If we make use of the topographic dispersion relation, we can relate the period to the bottom slope and stratification to give

$$r = \left(\frac{2Q_2}{\alpha N h}\right)^{1/2}. \tag{7}$$

The length scale of the eddies decreases with increasing bottom slope (plotted in Fig. 15c), and increasing stratification, and increases with increasing transport. The thickness of the eddies h could, in principle, be related to the potential vorticity of the outflow water. We find, however, that potential vorticity is not conserved very well downstream of the sill because of the subgrid-scale mixing. Rather than predict h we simply take the observed h downstream of the sill from the model fields. The estimate of the eddy diameter calculated from (7) with $Q_2 = 0.2 \times 10^6\ \mathrm{m^3\ s^{-1}}$ (the actual midlevel outflow, not the source strength), $h = 250$ m, and $N = 10^{-3}\ \mathrm{s^{-1}}$ compares closely with the eddy scales found in the model (Fig. 15c).

The kinetic energy of the midlevel outflow eddies is also strongly influenced by the bottom topography, as indicated by the maximum eddy kinetic energy downstream of the sill in layer 2 shown in Fig. 15d. An areal-averaged estimate of the eddy kinetic energy shows essentially the same dependence on bottom slope. The strength of the eddy kinetic energy increases from small values for weak topographic slopes to a maximum near $\alpha = 0.02$ and it then rapidly decays for further increases in bottom slope. The initial increase in eddy strength with increasing slope results from two mechanisms. The strength of the eddies is proportional to their potential vorticity anomaly relative to the ambient water over the slope. The potential vorticity anomaly of the midlevel outflow water arises because the thickness of the water that flows over the sill is much less than the thickness of the ambient water in the southern basin of the same density. This difference increases with increasing bottom slope, thus giving rise to stronger potential vorticity anomalies in the mid layer. The strength of the eddies

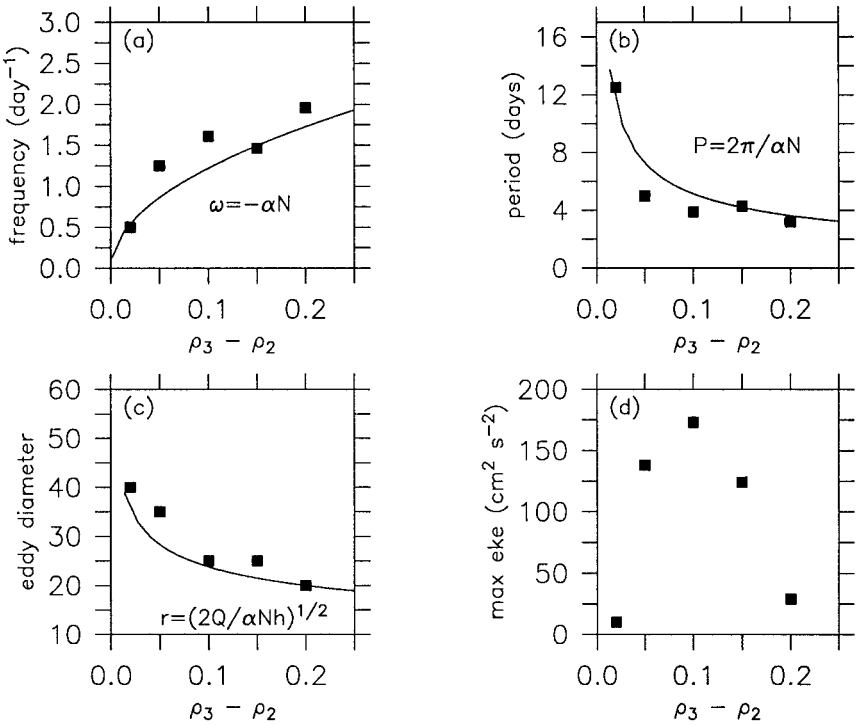

FIG. 16. Eddy characteristics as a function of the density change between the upper and lower overflows: (a) frequency of eddy formation and (b) period of eddy formation (the solid lines indicate the short topographic Rossby wave dispersion relation); (c) eddy diameter, the solid line is the diameter predicted by relation (7); and (d) maximum eddy kinetic energy.

is also inversely proportional to their horizontal length scale (for a given potential vorticity anomaly). As was seen in Fig. 15b, the length scale decreases with increasing bottom slope, also contributing to stronger eddies at larger slopes.

The eddy energy decays for very strong slopes because the vertical scale height of the perturbations, D, decreases with decreasing wavelength λ according to

$$D \propto H \exp\left(\frac{-2\pi L_d}{\lambda}\right), \tag{8}$$

where L_d is the horizontal deformation radius, and H is the total depth of the fluid (Pedlosky 1979). As the horizontal scale of the perturbations decreases, the vertical scale over which the perturbations extend also decreases. Eddies that are smaller than the deformation radius, $\lambda \leq 2\pi L_d$, will be strongly bottom trapped, and not well resolved in the present model.

Two additional influences may also be contributing to the decrease in energy for strong slopes. The angle at which the dense bottom current descends the slope increases with increasing bottom slope (and increasing stratification, see next section). For sufficiently rapid descent, the dense current can separate from the near coastal region where the high potential vorticity water exists before the midlevel flow can develop a cyclonic circulation (an inertial period). In addition, the timescale for subgrid-scale mixing to erode the cyclonic eddies also decreases as the eddy scale decreases, further contributing to the decrease in eddy energy for these cases.

b. Dependence upon the stratification

The density difference between the outflow layers also influences the characteristics of the variability downstream of the sill (Fig. 16). The frequency of the eddies increases approximately as the square root of the density difference between layers 2 and 3, consistent with the frequency of the short-wave topographic dispersion relation being proportional to the Brunt–Väisälä frequency $N = (g'/h)^{1/2}$. The length scale of the eddies decreases slightly for increasing stratification, approximately consistent with the mass flux constraint of (7) given by the solid line.

The eddy kinetic energy initially increases with increasing stratification and then rapidly decays to nearly zero for a density change of 0.2 kg m^{-3}. The initial increase is caused by the stronger velocity shear that results from the larger density change between the two outflow layers for a fixed potential vorticity anomaly. However, as the stratification increases, and the length scale of the eddies decreases the eddy energy drops off, this is consistent with the bottom trapping implied by (8) and the decoupling effect for steep plume descents.

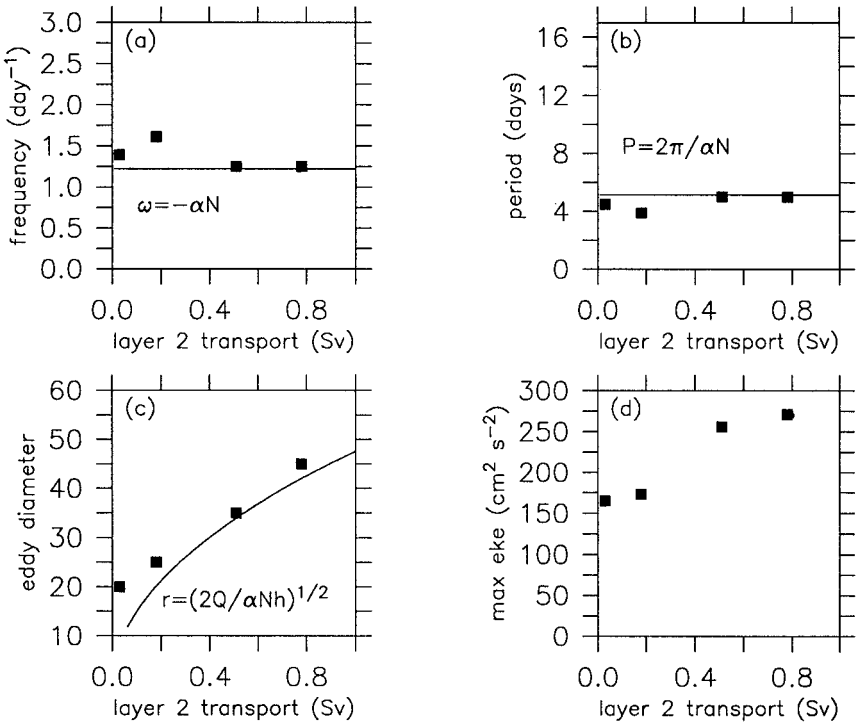

FIG. 17. Eddy characteristics as a function of the outflow transport in layer 2: (a) frequency of eddy formation and (b) period of eddy formation (the solid lines indicate the short topographic Rossby wave dispersion relation); (c) eddy diameter, the solid line is the diameter predicted by relation (7); and (d) maximum eddy kinetic energy.

c. Dependence upon the midlevel outflow transport

The eddy diameter increases with increasing midlevel outflow transport (Fig. 17c), in general agreement with the total mass flux constraint (7). The frequency of eddy formation, on the other hand, is independent of the strength of the outflow (Figs. 17a and 17b), as it should be if the propagation speed of the eddies is controlled by the topographic Rossby wave dispersion relation. On the other hand, calculations show that the eddy characteristics (frequency, diameter) are not strongly influenced by increases in the amount of dense water formed in layer 3 (although some amount is required, as previously discussed). This result suggests that the frequency and diameter of midlevel cyclones generated through this process could be used to estimate the transport in the midlevel outflow but that there is no direct relationship between the eddy characteristics and the transport in the dense overflow layer.

It is important to note that in most of these cases the primary source for the high potential vorticity water was the outflow, and not the bottom topography and initial condition, the exception being when the outflow transport is very low (the eddy diameter does not go to zero as the transport goes to zero in Fig. 17c). In the latter case, the length scale of the eddies will scale with the deformation radius and not with the volume transport as found here [Eq. (7)].

d. Sensitivity to other parameters

The qualitative behavior discussed above has been found to be insensitive to several other parameters in the model configuration. For example, the density change between the upper and mid outflow layers was found not to influence the behavior of the outflow significantly. The addition of a fourth outflow layer (density greater than ρ_3) did not strongly influence the formation of the cyclones. The fourth layer flows downslope quickly upon entering the basin and does not get spunup into cyclones as layer 3 does in the central case. This rapid draining of a thin bottom layer is similar to that seen in laboratory experiments discussed by LSB.

Free-slip boundary conditions for the horizontal momentum result in qualitatively similar cyclogenesis, although the variability in the immediate vicinity of the sill is then much larger. The free-slip boundary condition also reduces the effective bottom drag because the sidewall drag terms that are introduced at the bottom for steeply sloping bottom topography are eliminated [Eq. (4)], resulting in a reduced angle of descent for the dense overflow. The coupling mechanism discussed previously is still effective, however, though the cyclonic eddies emerge farther downstream as described in section 4b(1). We have not attempted to tune the subgrid-scale mixing parameterizations to give the least possible dissipation, although we know that lower values are

possible (numerically) and result in larger values of eddy kinetic energy, especially near the sill and downstream of the sill when the eddy radius is smallest.

We have also allowed a sloping bottom along the western boundary at depths less than the sill depth (the central cases all have a vertical wall along the western boundary down to the top of the sill). This supresses the strong variability downstream of the sill (but does not eliminate it) because the midlevel outflow and the dense overflow waters are displaced in the east–west direction such that they are partially decoupled. In this case, the midlevel outflow flows to the south as a western boundary current and the dense overflow descends the sloping topography as though there was no midlevel outflow. This result is entirely consistent with the coupling mechanism discussed above. The actual outflow in Denmark Strait does have a sloping topography along the western boundary at the sill, although most of the midlevel outflow is still observed to be directly over the dense overflow as they pass over the sill (necessary component to the PV outflow hypothesis). The outflow configuration in Denmark Strait is consistent with the outflow in our central cases that produce the strong variability, although the physical processes responsible for this flow structure are probably not properly represented in our model. The observations indicate a significant barotropic component in the outflow, probably as a consequence of wind forcing on the larger scale and the fact that Denmark Strait is located on the western boundary. The inability of our model to reproduce this flow structure with sloping topography along the shallow western boundary probably relates to our idealized forcing, limited vertical resolution, and neglect of the large-scale circulation.

A calculation was done in which the bottom topography was set to be the same as the mean interface depth between layers 2 and 3 in the central calculation, and the deep-water formation was shut off. The resulting outflow does not form any cyclones and looks essentially the same as the case with no deep-water formation and a uniformly sloping bottom (Fig. 11). This suggests that the pressure gradient associated with a dynamically active deep layer, and not simply some steering effect of the interface between layers 2 and 3, is important to the eddy formation process, consistent with the offshore advection mechanism outlined above.

6. Other models of density currents

The eddy variability in Denmark Strait has been the object of several previous modeling studies, starting with Smith's (1976, hereafter S76) seminal contribution in which he argued that a baroclinic instability of a uniform channel flow was the main source for mesoscale variability in Denmark Strait. Recently Jiang and Garwood (1996, hereafter JG96) modeled the descent of a density current injected onto a continental shelf and they too concluded that a form of baroclinic instability was the source of mesoscale variability. Laboratory studies have also been used to study the formation of eddies within density currents (Smith 1977; Griffiths 1983; Whitehead et al. 1990; LSB) and they show that a variety of seemingly unrelated processes can produce cyclones on sloping bottoms. There are similarities and some important differences between these calculations and experiments and the present modeling results that we will point out and attempt to explain, where we can. Our assumption is that the previous work is entirely correct; the only issue is applicability to the phenomenon in Denmark Strait, which, owing to the accumulation of observations, we now know much better than we did only a few years ago (reviewed in section 1b).

It is easy to point out one qualitative difference between ours and previous work: none of the previous studies have accounted for the multilevel outflow and three-dimensional nature of the potential vorticity field that actually occurs within Denmark Strait. Since this multilevel outflow has been found to be the primary agent for cyclogenesis in our model calculations, then this study is bound to be different from its predecessors, which all assumed that the outflow occurred in the overflow layer only. In that respect, the previous studies did not distinguish the Denmark Strait outflow, which we contend is highly energetic (section 1), from other single layer overflows (through Faroe Bank Channel or the Strait of Gibraltar) that are much less so.

a. Baroclinic instability of a uniform shear flow

Despite this difference in the outflow configuration, some of our results are similar to those of the previous baroclinic instability models. In particular, the source of the eddy kinetic energy is the potential energy of the mean stratification in all of the models (we did not present an energy budget). The S76 model assumes that the outflow is confined within a channel along which the mean shear and the bottom slope are uniform. The shear flow and the topography in Denmark Strait are highly variable in the direction of flow, and thus the choice of parameters is problematic. The stability of the shear flow depends upon the ratio of the isopycnal slope to the bottom slope and is unstable if this exceeds 1. S76 selected a rather large shear and a small bottom slope, in which case the most unstable wave has a period of several days, as is actually observed for the variability in Denmark Strait, and a wavelength of about 80 km, which is also reasonable. We suspect that the time and space scales are related by the topographic Rossby wave dispersion relation, which should be in common to all time-dependent models that include a sloping bottom and stratification.

In other respects the baroclinic instability model has what seem to be deficiencies when applied to Denmark Strait variability. Over most of the width of the Denmark Strait outflow the isopycnals in the overflow layer are nearly parallel with the bottom, which is not an unstable

configuration (see sections in Ross 1982). The overflow layer generally satisfies the necessary condition for baroclinic instability only on the offshore side of the current where the isopycnal interface slopes more steeply than the bottom topography by roughly 10% [deduced from inspection of sections in the Ross atlas (1982)]. The *e*-folding time for baroclinically unstable disturbances with 10% supercritical shear across the entire width of the flow is approximately 15 inertial periods, which is much longer than the growth rate of the cyclones observed in Denmark Strait (or in our model). The analysis of current meter data by S76 showed that the mesoscale variability in Denmark Strait exhibited little or no phase lag with depth, as we found here in our model results, while growing baroclinic waves require a substantial phase shift in the vertical. This seems to indicate that the Denmark Strait overflow downstream of the sill is not strongly baroclinically unstable. Finally, the linear S76 theory predicts a symmetric perturbation field with an equal number and amplitude of cyclones and anticyclones, while the present theory and the observations indicate a clear preponderance of cyclones. From all of this we conclude that while some important features of the S76 model are consistent with the observations—the time and length scales of the variability and that the source of the eddy energy is the mean potential energy—nevertheless baroclinic instability of a uniform channel flow does not appear to be the *primary* process that acts to generate mesoscale cyclones near the sill in Denmark Strait. (We note, however, that there may be other sources of mesoscale variability along the east coast of Greenland including baroclinic instability of the East Greenland Current and offshore generation of topographic Rossby waves.)

b. Baroclinic instability of density currents

Jiang and Garwood (1996) found that strong mesoscale eddies are produced just downstream of a dense plume injected onto a sloping bottom. They find upper-ocean cyclonic eddies overlying deep pulses of dense water over the slope. They attribute the source of the variability to a form of baroclinic instability described by Swaters (1991, hereafter SW91), who examined the baroclinic instability of a density current having a lens-like cross section. In such a current, the isopycnals will slope more steeply than the bottom slope on the offshore side of the lens, which is observed in many overflow currents including, at times, Denmark Strait as noted above. Thus, the Denmark Strait overflow may satisfy the necessary condition for instability locally (in the across-stream sense). [It should be noted that the Denmark Strait and all of the model configurations discussed here are not in the weakly sloping regime for which the analysis of SW91 is valid. The small parameter used in the Swaters asymptotic expansion solution is $s = \alpha L/H$, where α is the bottom slope, L is the horizontal length scale, and H is the fluid depth. For Denmark Strait parameters, $\alpha = 0.02$, $L = 50$ km, and $H = 800$ m, s is $O(1)$ and not small. Nor is it small in the JG96 case or the present one. In physical terms, the relative vorticity in the upper ocean in the SW91 model is controlled primarily by vortex stretching of the deep layer, while if s is $O(1)$ it is controlled by the change in bottom depth across the slope. Nonetheless, asymptotic solutions have often been found to successfully predict the qualitative behavior of systems well outside their formal regime of validity, so a comparison with our calculations and Denmark Strait seems warranted.]

As before, the linear instability model predicts an equal number of cyclonic and anticyclonic vortices above the overflow layer, which is quite different from the observations. The sense of the deep circulation in the model is observed to be cyclonic around the local maxima in the deep overflow layer thickness, as opposed to the anticyclonic circulation in SW91. The SW91 model and the JG96 calculations indicate much stronger variability on the offshore (deep) side of the overflow layer than on the onshore side and that the variability is stronger within the overflow than in the fluid above. Observations from Denmark Strait show a different distribution [the cyclones are strongest at depths well above the onshore side of the overflow water, section 1b(2)] that seems at odds with a source on the offshore side of the overflow layer.

This form of baroclinic instability is much less evident in our model calculations than it was in JG96 (and this is true even in the single dense overflow cases). Part of this difference may arise from the way in which the overflow current comes onto the slope; in our solutions the sill overflow is part of the solution (though we suspect not well resolved), while in JG96 it was specified as a plug flow. The stability of the overflow downstream of the sill is likely to be strongly influenced by the potential vorticity distribution carried downstream from the sill, and the dynamics near the sill probably merit greater attention than has been given here.

c. Laboratory experiments

Smith (1977) reported a series of laboratory experiments in which bottom currents were generated by injecting dense water onto a sloping bottom. In the low Ekman number regime, most relevant to Denmark Strait, he found that the bottom current broke up into a series of domes having strong cyclonic vortices overhead. For sufficiently large Ekman numbers (obtained by decreasing the source strength) no eddies were formed, and the flow was essentially steady to low frequency perturbations. The formation of cyclonic eddies in the low Ekman number regime appears to be much like the eddy formation process we find in our numerical model when there is a single overflow layer (section 4a), and as discussed further in this section. When bottom drag is increased in these experiments, analogous to the laboratory experiments with larger Ekman numbers, the

eddy formation may cease. While some bottom drag is evidently essential for causing the descent of the overflow layer and setting up the alongslope pressure gradient, nevertheless too much bottom drag, $C_D \geq 0.01$ is sufficient, can cause the overflow current to descend so rapidly that it essentially decouples from the middle layer and no eddies are formed.

Whitehead et al. (1990) described an ingenious series of laboratory experiments that demonstrated the very wide range of processes, including convection from ice cubes and mechanical mixing, that could cause eddy formation over a sloping bottom. The most relevent configuration was perhaps the injection of dense water onto a sloping bottom. Immediately downstream of the injection point, there is clearly a great deal of turbulent mixing and entrainment into the dense fluid, diminishing its density anomaly. Downstream of this strongly turbulent region, however, the dense water begins to flow parallel and then slowly down the topography in the form of a broad density current. If the jet was injected into shallow enough water, then the density current was found to break up into deep weak cyclones with strong cyclones in the overlying fluid, strongly suggestive of Denmark Strait. However, if the jet was injected into deeper water, then no such cyclones were formed and the bottom current continued down the topography in a nearly steady, broad current. Whitehead et al. (1990) attributed the cyclogenesis to turbulent entrainment of fresh water into the salty plume, similar to the mechanism proposed by Griffiths (1983).

Lane-Serff and Baines have recently carried out a similar series of laboratory experiments in which dense water flows over a weir and then downslope in a rotating tank. They investigate the characteristics of the eddies (size, frequency, strength) as a function of the strength of the Ekman number and bottom slope (among other things). They find a similar dominance of cyclonic eddies for weakly viscous regimes, while sufficiently strong viscosity could suppress eddy formations by draining away the dense fluid in the Ekman layer before the midlevel could develop cyclonic vorticity (an inertial period). The Denmark Strait, and our numerical experiments, are within the regime where strong eddies are formed. They find that the frequency of eddy generation scales with a stretching parameter that, with the appropriate change of variables, is equivalent to our interpretation of the frequency being controlled by the shortwave topographic dispersion relation. They also identify the source of the cyclonic vorticity as the essentially adiabatic stretching of the water initially present over shallow topography.

We believe that these mid- or upper-level cyclones, and also those found in the JG96 calculations, may have been formed by the adiabatic advection process described in section 5. That is, the coupling between the dense water and the upper fluid is achieved by the geostrophic offshore flow required to balance the alongshore pressure gradient and that the potential vorticity gradient supplied by the bottom topography (i.e., as part of the initial condition) provides the source for the high potential vorticity cyclones. The evidence that this is the primary cyclogenesis process is that these cyclones formed only when the jet was injected into shallow water (where a strong gradient in potential vorticity exists overhead) and descended the slope at weak angles and not when injected into deeper water or when subject to very rapid topographic descent. The mechanics of this cyclogenesis process is very much like the one we have called PV outflow, the only difference being the source of the high potential vorticity water. These laboratory experiments are analogous to the model calculations with a dense overflow only and where it was found that cyclones emerge only when the dense plume enters the southern basin in the vicinity of a thin midlayer thickness (Figs. 12 and 14b) and when the bottom drag was not extremely large.

7. Closing

We have examined some aspects of the remarkable mesoscale variability observed in Denmark Strait. This variability has been the subject of several previous laboratory, numerical, and field studies, but it should be clear from the present study that there is a great deal left to be learned. Laboratory studies that include comprehensive measurements of circulation could be used to investigate cyclogenesis mechanisms, and numerical models more complete than ours could be used to investigate the effects of the large-scale circulation (particularly the barotropic mode) and realistic bottom topography. Field studies in Denmark Strait are particularly challenging, given the rapid temporal variability, but are, of course, essential for defining the structure of the mesoscale variability. It would be most valuable to observe the formation and the initial propagation of a cyclone, and to test whether cyclones are indeed the dominant mode of variability. In the long run we need to know how mesoscale variability may affect the exchange between the Norwegian–Greenland Sea and the North Atlantic, and whether it affects the product water properties of the Denmark Strait outflow. This study makes a start in that direction, we hope, by developing a new idea regarding the generation mechanism.

a. Summary

To summarize the present results we revisit the questions raised in the opening section.

1) What is the source of the mesoscale *variability* in Denmark Strait? Our hypothesis is that the dominant generation process is an adjustment of the high PV outflow water column to the low PV oceanic environment. This adjustment includes substantial stretching of the midwater column (Arctic Intermediate Water level). Numerical experiments show that the stretching mechanism produces intense, discrete mesoscale cyclones that have

the time and space scales of short topographic waves. These cyclones carry nearly all of the southward going transport of the intermediate level. Strong variability is found in both the lower and intermediate layers, although the source of the variability is the stretching of the intermediate layer. Numerical experiments show that the necessary ingredients for the development of strong eddies are (i) a dense bottom current that descends a topographic slope and (ii) a potential vorticity gradient in the water overlying the dense bottom current.

The PV outflow hypothesis together with the numerical simulations seem to account for most of the known characteristics of these cyclones (Table 1). The most telling qualitative observations are that (i) most of the observed mesoscale variability is associated with intense cyclones and (ii) the cyclones have a middepth maximum and carry a remnant of Arctic Intermediate Water in their core. Some quantitative measures also compare well, for example, the eddy size and intensity, however the frequency of eddy formation in the central case is a little low, as is the eddy translation speed, probably due to the lack of a realistic basin-scale southerly flow of $O(10\ \text{cm s}^{-1})$ along the western boundary of the ocean.

2) Why is the Denmark Strait outflow especially energetic? The outflow through Denmark Strait appears to be unique in that the entire water column outflows and the intermediate layer has anomalous (high) PV with respect to the open ocean. Other major overflows (e.g., through Faroe Bank Channel and the Strait of Gibraltar) are the lower layer of a two-layer exchange flow and consist of nearly homogeneous layers (low PV) that are denser than the immediate oceanic environment. Numerical experiments indicate that such overflows can be somewhat time dependent, but that they are qualitatively different from the multilevel outflow through Denmark Strait. To our knowledge, these other overflows do not exhibit the kind of intense and continuous mesoscale variability found just downstream of the sill in Denmark Strait. [These overflows are, of course, time variable, though in different ways. For example, the Mediterranean overflow is strongly modulated by tides within the Strait of Gibraltar. Several hundred kilometers downstream of the sill the mixed Mediterranean overflow water becomes neutrally buoyant in the lower main thermocline where it retains a low PV core. An appreciable fraction of the mixed overflow water forms into anticyclonic eddies, or meddies (Prater and Sanford 1994).]

b. Remarks

We have described the generation process as an *adjustment* of the outflow water column rather than as an *instability* of a mean flow. The latter description would also be appropriate in that steady forcing and steady boundary conditions result in a time-dependent (numerical) solution. It would be natural and fruitful to view the process as an instability, except that we have never produced a steady flow when there were two or more outflow layers. Hence we have not emphasized stability per se. Pichevin and Nof (1997) concluded that for some flow configurations eddy formation is a necessary component of the adjustment process for a single layer flowing through a narrow channel into a quiescent ocean. That we do not find a steady solution in our numerical solutions suggests that, if a steady solution exists, then it is probably highly unstable due to the abrupt change in the background potential vorticity downstream of the sill. This hypothetical steady solution would probably not be the same as the temporal mean of the time-dependent solutions described here, given that most of the midlevel transport occurs in eddies. The source of the eddy energy is the potential energy associated with the outflow stratification, and the conversion process is certainly baroclinic (though the response is almost barotropic). It might thus seem appropriate to term the generation process a baroclinic instability. However, we have avoided that usage because the dynamics in this case are fundamentally different from that of the normal mode instability of a two-dimensional shear flow usually brought to mind by baroclinic instability. The background fields in this problem are three-dimensional, and the rapidly varying component of the flow and the bathymetry in the alongstream direction are of first importance. We are not aware of a stability analysis that can be applied to this flow configuration, but we anticipate that such an analysis would yield additional insight and might help connect this apparently singular problem to an extensive literature.

Acknowledgments. This research was supported by the National Science Foundation through Grants OCE-95-31874 to MS as part of the Atlantic Climate Change Experiment, and Grant OCE-94-01300 to JP. We thank John Bruce and two anonymous reviewers for their helpful suggestions.

REFERENCES

Baringer, M. O., and J. F. Price, 1997: Mixing and spreading of the Mediterranean outflow. *J. Phys. Oceanogr.,* **27,** 1654–1677.

Bleck, R., and L. T. Smith, 1990: A wind-driven isopycnic coordinate model of the North and Equatorial Atlantic Ocean. 1. Model development and supporting experiments. *J. Geophys. Res.,* **95**(C), 3273–3285.

——, C. Rooth, D. Hu, and L. T. Smith, 1992: Salinity-driven thermocline transients in a wind- and thermohaline-forced isopycnic coordinate model of the North Atlantic. *J. Phys. Oceanogr.,* **22,** 1486–1505.

Borenas, K. M., and P. Lundberg, 1988: On the deep-water flow through the Faroe Bank Channel. *J. Geophys. Res.,* **93,** 1281–1292.

Bruce, J. G., 1995: Eddies southwest of the Denmark Strait. *Deep-Sea Res.,* **42,** 13–29.

Cooper, L. H. N., 1955: Deep water movements in the North Atlantic as a link between climatic changes around Iceland and biological productivity of the English Channel and Celtic Sea. *J. Mar. Res.,* **14,** 347–362.

Crease, J., 1965: The flow of Norwegian Sea water through the Faroe Bank Channel. *Deep-Sea Res.,* **12,** 143–150.

Dickson, R. R., and J. Brown, 1994: The production of North Atlantic Deep Water: Sources, rates and pathways. *J. Geophys. Res.,* **99,** 12 319–12 341.

Foldvik, A., T. Kvinge, and T. Torrenson, 1985: Bottom currents near the continental shelf break in the Weddell Sea. *Oceanology of the Antarctic Continental Shelf,* Antarctica Res. Ser., Vol. 43, 21–34.

Griffiths, R. W., 1983: Inertial wave drag and the production of intense vortices by turbulent gravity currents with implications for the sinking of bottom waters. *Ocean Modelling* (unpublished manuscript), **50,** 9–12.

Heezen, B. C., and G. L. Johnson, 1969: Mediterranean under-current and microphysiography west of Gibraltar. *Bull. Inst. Oceanogr., Monaco,* **67,** 1–95.

Jiang, L., and R. W. Garwood, 1996: Three-dimensional simulations of overflows on continental slopes. *J. Phys. Oceanogr.,* **26,** 1214–1233.

Johnson, G. C., T. B. Sanford, and M. O. Baringer, 1994: Stress on the Mediterranean outflow plume. Part I: Velocity and water property measurements. *J. Phys. Oceanogr.,* **24,** 2072–2083.

Killworth, P. D., 1983: Deep convection in the world ocean. *Rev. Geophys. Space Phys.,* **21,** 1–26.

Krauss, W., 1996: A note on overflow eddies. *Deep-Sea Res.,* **43,** 1661–1667.

Lane-Serff, G. F., and P. G. Baines, 1998: Eddy formation by dense flows on slopes in a rotating fluid. *J. Fluid Mech.,* in press.

Lozier, M. S., W. B. Owens, and R. G. Curry, 1995: The climatology of the North Atlantic. *Progress in Oceanography,* Vol. 36, Pergamon, 1–44.

Mauritzen, C., 1996: Production of dense overflow waters feeding the North Atlantic across the Greenland–Scotland Ridge. Part 1: Evidence for a revised circulation scheme. *Deep-Sea Res.,* **43,** 769–806.

McWilliams, J. C., 1988: Vortex generation through balanced adjustment. *J. Phys. Oceanogr.,* **18,** 1178–1192.

Pedlosky, J., 1979: *Geophysical Fluid Dynamics.* Springer-Verlag, 624 pp.

Pichevin, T., and D. Nof, 1997: The momentum imbalance paradox. *Tellus,* **49A,** 298–319.

Poulain, P. M., A. Warn-Varnas, and P. P. Niiler, 1996: Near-surface circulation of the Nordic Seas as measured by Lagrangian drifters. *J. Geophys. Res.,* **101** (C8), 18 237–18 258.

Prater, M. D., and T. B. Sanford, 1994: A meddy off Cape St. Vincent. Part 1: Description. *J. Phys. Oceanogr.,* **24,** 1572–1586.

Price, J. F., and M. O'Neil Baringer, 1994: Outflows and deep water production by marginal seas. *Progress in Oceanography,* Vol. 33, Pergamon, 161–200.

——, ——, R. G. Lueck, G. C. Johnson, I. Ambar, G. Parilla, A. Cantos, M. A. Kennelly, and T. B. Sanford, 1993: Mediterranean outflow mixing and dynamics. *Science,* **259,** 1277–1282.

Ross, C. K., 1982: Overflow '73—Denmark Strait: Vol 3—Temperature, salinity and sigma-t sections. Canadian Tech. Rep. of Hydrography and Ocean Sciences 16, Bedford Institute of Oceanography, Dartmouth, NS, Canada. [Available from Bedford Institute of Oceanography, P.O. Box 1006, Dartmouth, Nova Scotia B2Y 4A2, Canada.]

——, 1984: Temperature–salinity characteristics of the ''overflow'' water in Denmark Strait during ''OVERFLOW '73.'' *Rapp. P.-V. Reun.—Cons. Int. Explor. Mer.,* **185,** 111–119.

Saunders, P. M., 1990: Cold outflow from the Faroe Bank Channel. *J. Phys. Oceanogr.,* **20,** 29–43.

Smagorinsky, J. S., 1963: General circulation experiments with the primitive equations. I: The basic experiment. *Mon. Wea. Rev.,* **91,** 99–164.

Smith, P. C., 1976: Baroclinic instability in the Denmark Strait overflow. *J. Phys. Oceanogr.,* **6,** 355–371.

——, 1977: Experiments with viscous source flows in rotating systems. *Dyn. Atmos. Oceans,* **1,** 214–272.

Swaters, G. E., 1991: On the baroclinic instability of cold-core coupled density fronts on a sloping continental shelf. *J. Fluid Mech.,* **224,** 361–382.

Warren, B. A., 1981: Deep circulation of the world ocean. *Evolution of Physical Oceanography, Scientific Surveys in Honor of Henry Stommel,* B. A. Warren and C. Wunsch, Eds. The MIT Press, 6–14.

Whitehead, J. A., 1989: Giant ocean cataracts. *Sci. Amer.,* **260,** 50–57.

——, M. E. Stern, G. R. Flierl, and B. A. Klinger, 1990: Experimental observations of baroclinic eddies on a sloping bottom. *J. Geophys. Res.,* **95,** 9585–9610.

Worthington, L. V., 1969: An attempt to measure the volume transport of Norwegian Sea overflow water through the Denmark Strait. *Deep-Sea Res.,* **16,** 421–432.